

Development and Characterization of Sulfonated Polyimide Membrane for Proton Exchange Membrane Fuel Cell Applications

by

Hai Zheng

A thesis submitted to the Graduate Faculty of
Auburn University
in partial fulfillment of the
requirements for the Degree of
Master of Science

Auburn, Alabama
December 13, 2010

Keywords: fuel cell, synthesis, characterization, SPI copolymer,
proton exchange membrane

Copyright 2010 by Hai Zheng

Approved by

Sabit Adanur, Chair, Professor of Polymer and Fiber Engineering
Peter Schwartz, Professor of Polymer and Fiber Engineering
Gwynedd A. Thomas, Associate Professor of Polymer and Fiber Engineering

Abstract

The developments of the proton exchange membrane fuel cells are introduced and synthesis and characterization of new sulfonated polyimides are described. 1,4,5,8- naphthaene-tetracarboxylic dianhydride (NTDA), 4,4'- iaminostilbene - 2,2'- disulfonic acid (DSDSA), and other common diamines, such as 4,4'- oxydianiline (ODA), and 4,4'- methylene dianiline (MDA) were used to synthesize the sulfonated polyimide copolymer by using a one-step high temperature polymerization method. The sulfonation degree of the copolymers can be controlled by using different molar ratio of DSDSA to the common diamines. Flexible, brown-colored and mechanically strong membranes were successfully obtained. The membranes were characterized with Fourier transform infrared spectra, thermogravimetric analysis, differential scanning calorimetry, water uptake, ion-exchange capacity, proton conductivity measurements and mechanical tests. These results showed that the membranes had good thermal and mechanical stability and exhibited good performance when they were assembled into membrane electrode assemblies (MEAs). Fuel cell testing was performed. The SPI copolymer based MEA was tested under different hydrogen flow rates; it was also compared with the commercial Nafion® based MEA. The SPI membrane exhibited good performance compared to Nafion®.

Acknowledgments

First of all, I would like to express my gratitude to Dr. Sabit Adanur, my advisor for providing me the opportunity to pursue my master degree in Auburn University, leading me to the field of fuel cell and giving me a lot of valuable advice in academic field. I want to thank my committee members, Dr. Peter Schwartz and Dr. Gwynedd A. Thomas for their contribution. Special thanks to Mr. Steve Howard, Dr. Ramsis Farag and Dr. Wei Liu for their kindly help in the lab.

I wish to extend my thanks to all my friends and colleagues for the joy and fun they brought to me. Good studying and working atmosphere at the department of Polymer and Fiber Engineering also help me feel comfortable everyday in Auburn University. The research was supported by the U.S. Department of Commerce (DOC-ITA-06-3112-0), which is appreciated.

Finally, I would like to express my love to my dear parents, sincerely. Thank you for all the inspiration you have given me.

Table of Contents

Abstract.....	ii
Acknowledgments.....	iii
List of Tables	vii
List of Figures.....	viii
List of Abbreviations	xi
Chapter One Introduction	1
Chapter Two Literature Review.....	3
2.1. Mechanism of the PEMFC.....	3
2.2. Proton Exchange Membrane (PEM)	5
2.3. Theory of Proton Transfer in the Proton Exchange Membrane	8
2.4. Sulfonated Polyimide Copolymer (SPI).....	9
2.5. Membrane Electrode Assembly (MEA).....	15
2.6. Catalyst Layer (CL).....	17

2.7. Gas Diffusion Layer (GDL)	18
Chapter Three Manufacturing and Characterization of SPI Copolymer Based Proton Exchange Membrane.....	
3.1. Materials Used.....	19
3.2. Synthesis of DSDSA-based SPI Copolymers	21
3.3. Membrane Manufacturing.....	22
3.4. Polymer and Membrane Characterization.....	23
3.4.1. FTIR Analysis.....	26
3.4.2. Thermogravimetric Analysis (TGA)	27
3.4.3. Differential Scanning Calorimetry (DSC).....	29
3.4.4. Water Uptake.....	30
3.4.5. Ion Exchange Capacity (IEC).....	31
3.4.6. Proton Conductivity Measurement.....	32
3.4.7. Mechanical Tests	34
Chapter Four Manufacturing of the SPI Membrane Based Membrane Electrode Assembly and Testing the Fuel Cell	
4.1. Preparation of the MEA	38
4.2. Assembly of the Fuel Cell.....	39
4.3. Fuel Cell Testing	43

Chapter Five Future Developments in Synthesizing	51
5.1. In Situ Technique	51
5.2. Post-sulfonation.....	53
5.3. Cross-linking Reaction.....	54
5.4. Automatic Solution Casting	55
Chapter Six Conclusions	58
References	59

List of Tables

Table 1. Materials used to produce the SPI based membrane	19
Table 2. Raw data of the SPI membrane tensile tests	34
Table 3. Data for Nafion® tensile tests.....	36
Table 4. SPI membrane tear test data.....	37

List of Figures

Figure 1. Schematic of the proton exchange membrane fuel cell (PEMFC) principle.....	4
Figure 2. Chemical structure of Nafion®	5
Figure 3. Chemical structure of alternative sulfonated polymers.....	7
Figure 4. Chemical structure of acid-base complex membranes	7
Figure 5. Modeling of the proton transfer in proton exchange membrane	8
Figure 6. Chemical structure of polyimide	10
Figure 7. A five-membered ring sulfonated polyimide containing phosphine oxide	13
Figure 8. A sulfonated six-membered ring polyimide based on BDA, ODA, and NDA	14
Figure 9. Main components of PEMFC.....	15
Figure 10. Main components of MEA	16
Figure 11. Cost of fuel cell stack in 2008	17
Figure 12. Chemical reaction for synthesis of SPI	22
Figure 13. SPI copolymer membrane	23
Figure 14. Nicolet 6700 FT-IR spectrometer.....	24
Figure 15. DSC Q2000 TA instrument.....	24

Figure 16. TGA Q500 instrument.....	25
Figure 17. Instron machine	25
Figure 18. FTIR testing of the ODA based diamine SPI membrane	27
Figure 19. TGA testing of the SPI membrane	28
Figure 20. DSC testing of the SPI membrane.....	30
Figure 21. Schematic of the membrane proton conductivity measurement.....	33
Figure 22. Load versus tensile strain curves of the SPI membrane samples	35
Figure 23. Dimensions of SPI membrane sample for tearing test	37
Figure 24. SPI membrane based MEA	39
Figure 25. Graphite plate with U-shape runner	40
Figure 26. Graphite plate with linear runner.....	40
Figure 27. PVC end plate with Nickel current collector.....	41
Figure 28. Components of the fuel cell before assembling	42
Figure 29. Schematic of the manufactured PEMFC	42
Figure 30. Testing of the SPI membrane based fuel cell	44
Figure 31. Voltage versus time curves of the SPI based fuel cell.....	44
Figure 32. Voltage versus time curves of the SPI based fuel cell under two different H ₂ flow rates.....	45
Figure 33. Voltage versus time curves of the SPI based fuel cell with hydrogen disconnected under two different H ₂ flow rates.....	46
Figure 34. Voltage versus time curves of the Nafion® based fuel cell under two different H ₂ flow rates.....	47

Figure 35. Voltage versus time curves of the Nafion® based fuel cell with hydrogen disconnected under two different H ₂ flow rates.....	48
Figure 36. Voltage versus time curves of the fuel cells with different MEAs under the same hydrogen flow rate	49
Figure 37. Voltage versus time curves of the fuel cells with different MEAs with hydrogen disconnected under the same hydrogen flow rate	49
Figure 38. I&J4000-LF RoHs bench top dispensing industrial robot.....	57
Figure 39. The nozzle in the dispensing industrial robot.....	57

List of Abbreviations

AFC Alkaline Fuel Cell

CL Catalyst Layer

DS Degree of Sulfonation

DSC Differential Scanning Calorimetry

DSDSA 4, 4'-Diaminostilbene-2, 2'-Disulfonic Acid

FT-IR Fourier Transform Infrared Spectroscopy

GDL Gas Diffusion Layer

HTPEM High Temperature Proton Exchange Membrane

IEC Ion-Exchange Capacity

MCFC Molten Carbonate Fuel Cell

MD Machine Direction

MDA 4, 4'-Diaminodiphenylmethane

N Newton

NTDA 1, 4, 5, 8-Naphthalenetetracarboxylic Dianhydride

ODA 4, 4'-Oxydianilin

PAFC Phosphoric Acid Fuel Cell

PEM Proton Exchange Membrane

PEMFC Proton Exchange Membrane Fuel Cell

PFSAM Perfluorinated Sulfonic Acid Membranes

PI Polyimide

PPA PolyPhosphoric Acid

PTFE Polytetraflouroethylene

RH Relative Humidity

SOFC Solid Oxide Fuel Cell

TD Transverse Direction

TGA Thermogravimetric Analysis

Chapter One

Introduction

There is no wonder that the Industrial Revolution has played an important role on the glorious developments by mankind. Great movements in the history of human beings are led by the discovery and application of the electrical energy.

In July 1752, Benjamin Franklin, an American scientist, attracted lightning in a kite experiment, so that people realized that lightning is electricity. In 1786, Italian scientist Galvani found out that the frog leg cramped between two different metals. He thought that was a bio-electrical phenomenon. In 1791, Volta got interested in this phenomenon, made a series of experiments, and published a paper in 1793. Later, through further experimental studies, Volta discovered that two different metals can have power generation. As a result, battery was invented, which was also called volt generator. The invention of volt battery allowed scientists to use relatively stable large electrical currents at various studies.

In 1839, Judge William Robert Grove explained the possibility of generating electricity by the reaction of hydrogen and oxygen. He established that, when running an electric current through water, water would split into hydrogen and oxygen. He reckoned that, if it worked one way, it should also work in reverse. To prove his theory, Grove built the first “fuel cell” in the world.

In 1866, German engineer Siemens, invented strong generators, and used them in locomotives.

A fuel cell is an electrochemical conversion device. It converts the chemical energy (Source: H_2) into electric energy directly without any other reaction, i.e., it does not follow the Carnot cycle [1], which means the ratio of energy conversion is high. Hydrogen is an outstanding carrier of energy. When it is burnt, it turns into water, which can be again split into hydrogen and oxygen, forming a “green” cycle.

Although the fuel cell was invented in 1839, its true potential in commercial applications was not realized until the 1960s. With the highly developed economy and industry, global warming, greenhouse effects, environmental pollution and smog have become a concern. It should be noted that these changes in our environment are, in varying degrees, the result of our own human activities. It is our established industry system, traffic system, and housekeeping system that bring so much pollution to our environment. Therefore, more attention is being paid to development of fuel cells to fit people’s needs better. Just by searching the National Energy Policy Act in 2005, more than 100 results related to the fuel cells can be obtained, which include hybrid vehicles, fuel cell buses, micro fuel cells and gasification fuel cells. [2]

Basically, there are five distinct fuel cell types: alkaline fuel cell (AFC), molten carbonate fuel cell, phosphoric acid fuel cell (PAFC), proton exchange membrane fuel cell (PEMFC) and solid oxide fuel cell (SOFC). However, these fuel cells require very expensive materials and could only be used for stationary applications due to their size except the PEMFC. Therefore, the PEMFC has become the best choice among them for the future, to provide both stationary and mobile green and renewable energy without any noise.

Chapter Two

Literature Review

2.1. Mechanism of the PEMFC

The following section is a brief review, related to the structure and electrochemical principles of the most common proton exchange membrane fuel cell - hydrogen–oxygen proton exchange membrane fuel cell.

Generally speaking, a hydrogen–oxygen proton exchange membrane fuel cell consists of one anode (the electrode on the hydrogen side), one cathode (the electrode on the oxygen side) and one proton-conducting polymer membrane (the electrolyte) which separates the anode and cathode sides. This was called a "solid polymer electrolyte fuel cell" (SPEFC) in the early 1970s, before the proton exchange mechanism was well-understood [3].

On the anode, electrically neutral hydrogen molecules, which are stored in a hydrogen tank, are oxidized through electron donation into hydrogen ions (Figure 1). These positively charged hydrogen ions pass through the polymer membrane towards the negatively charged cathode. The membrane has such properties that hydrogen ions, also known as protons, can diffuse through it but the larger oxygen ions do not (hence the name proton exchange membrane).

The reaction in anode: $\text{H}_2 \rightarrow 2\text{H}^+ + 2\text{e}^-$

In the cathode, the hydrogen ions react with the oxygen from the air and the electrons that are provided by the current collector leading to the cathode. The reaction result is the formation of water. It is known that during electrolysis, it was necessary to put energy into the dissociation of water molecules; in contrast, energy is released during the recombination of the ions.

The reaction in cathode: $4\text{H}^+ + 4\text{e}^- + \text{O}_2 \rightarrow 2\text{H}_2\text{O}$

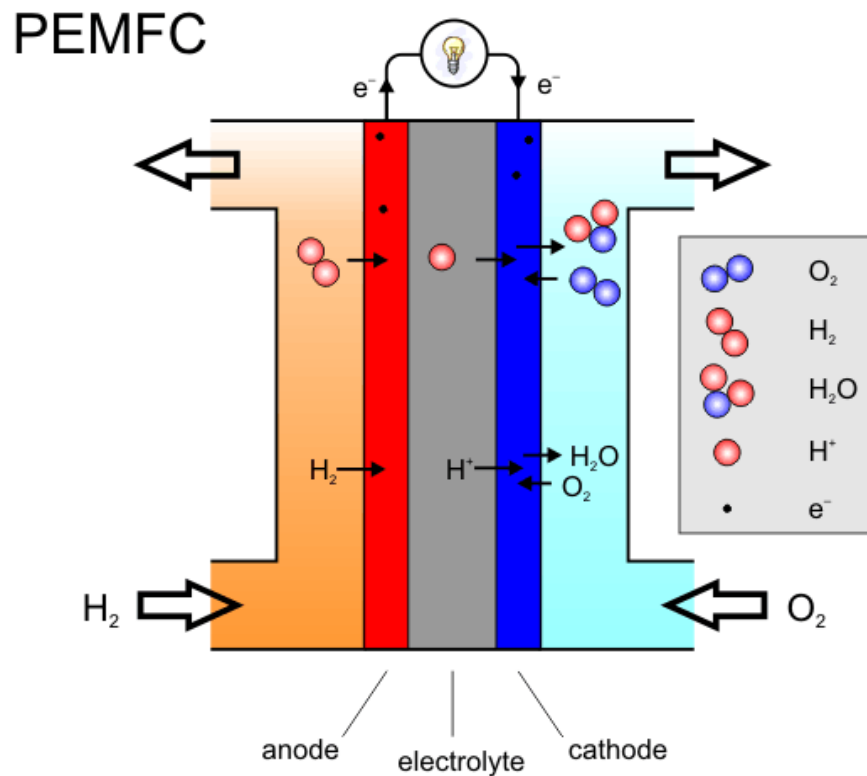


Figure 1. Schematic of the proton exchange membrane fuel cell (PEMFC) principle [4]

In this way, an electrical voltage is produced across the fuel cell. If an electrical load were connected to anode and cathode, e.g. a bulb, electrons flow from anode to cathode, in other words, an electric current flow and the bulb lights. [5]

2.2. Proton Exchange Membrane (PEM)

Proton exchange membranes are ionically conducting semi-permeable, plastic-like membranes, which are normally 50~175 micron thick, and therefore vulnerable. Typically, polymer membrane electrolytes play two major roles: 1. separating both fuel and oxidant apart to prevent mixing and 2. transporting protons from anode to cathode to complete the redox reaction.

There are several requirements for the physical properties of polymer membrane electrolyte: (1) ionic conductivity without electron conductivity, (2) good mechanical properties and flexibility in dry state, (3) gas impermeability, (4) chemical stability, (5) thermal and hydrolytic stability and (6) ability to form a thin film.

Currently, the most popular choice for PEMFC is the hydrated perfluorosulfonic polymers such as Dupont's patented- Nafion® series [6], which is a kind of sulfonated tetrafluoroethylene based perfluorosulfonic acid (PFSA) polymer membrane. Nearly all of the commercially available membranes are based on Nafion®. Nafion® also has the largest body of literature devoted to its study because of its demonstrated industrial importance and availability. Nafion® composite systems also have already become significant in both industrial and academic research.

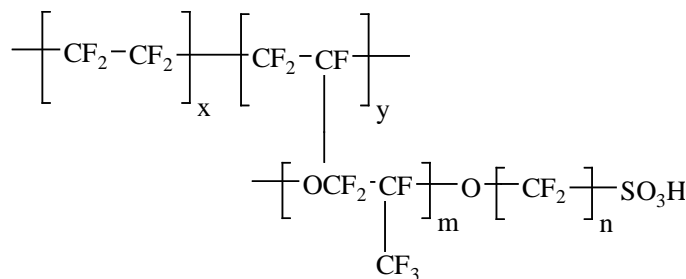


Figure 2. Chemical structure of Nafion®

PFSA membrane is composed of carbon-fluorine backbone chains with perfluoro side chains containing sulfonic acid groups, in which hydrogen ions are partially or totally exchanged by other cations or cationic groups. From the structure of Nafion® in Figure 2, its unique ionic conductivity can be readily explained: incorporating perfluorovinyl ether bonds provide the mechanical stability (flexibility), tetrafluoroethylene (Teflon®) backbone provides chemical stability, and the terminated sulfonate groups provide proton exchange pathway. However, all of these polyperfluorosulfonic acid membranes are expensive and suffer from the same shortcomings, namely, low conductivity at low water contents, relatively low mechanical strength at higher temperature, and moderate glass transition temperatures. These materials are not usable at high temperatures (over 120°C); therefore, it is an extremely urgent task for researchers to develop new proton exchanging membranes for commercial utilization. That's why several other PEM membranes based on other systems were developed for medium-high temperature operation, including modified PFSA membranes, alternative sulfonated polymers and their inorganic composite membranes (Figure 3) and acid-base complex membranes (Figure 4) [7]. This kind of PEM membrane is believed to be the main developing trend in the 21st century.

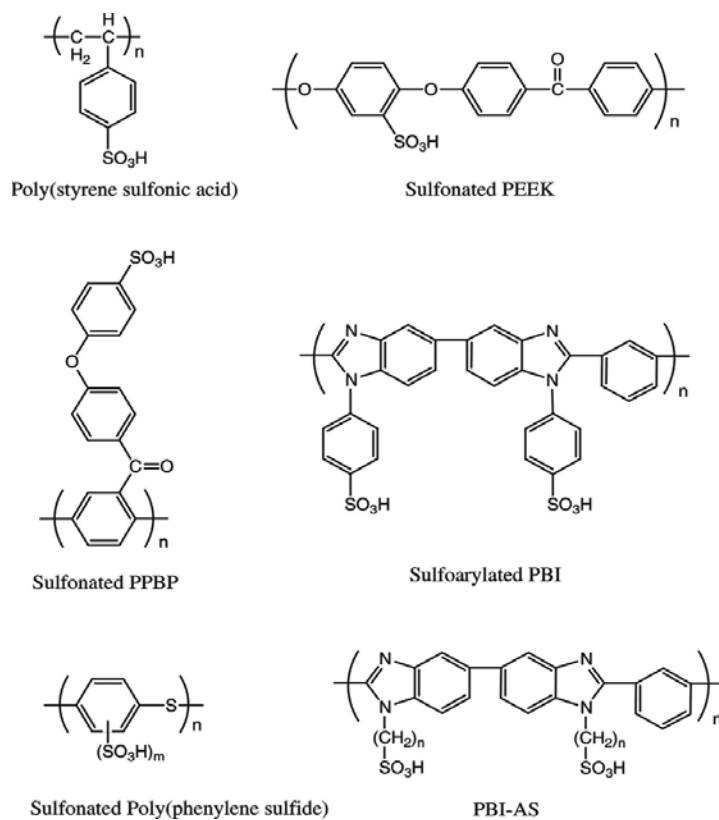


Figure 3. Chemical structure of alternative sulfonated polymers

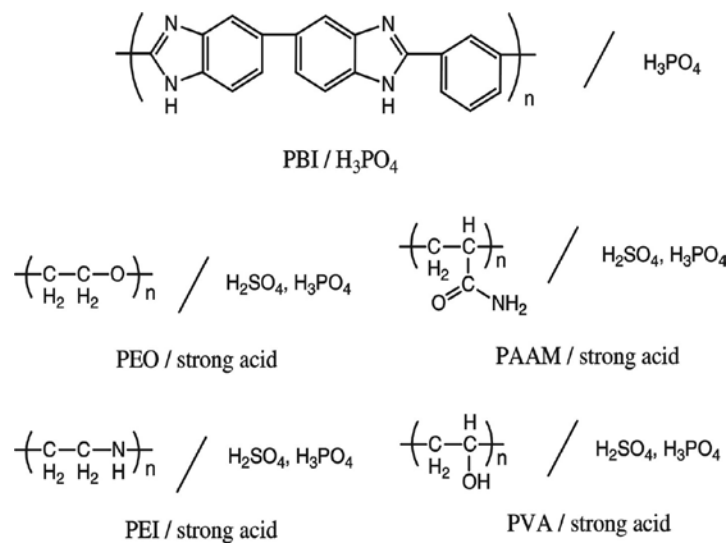


Figure 4. Chemical structure of acid-base complex membranes

2.3. Theory of Proton Transfer in the Proton Exchange Membrane

As mentioned before, normally the functional groups in the proton exchange membranes are the sulfonic acid groups. Proton transfer between sulfonic acid groups can be explained using theoretical approaches.

It was assumed that all SO_3H groups contain one hydrogen, such that the net charge of the system is zero (Figure 5c). It is considered that the movement of either an excess proton (Figure 5a, total charge + 1) or a deficit proton (proton hole, Figure 5b, total charge - 1) from one SO_3H group to another can take place via water molecules, that is called deprotonation and proton transport.

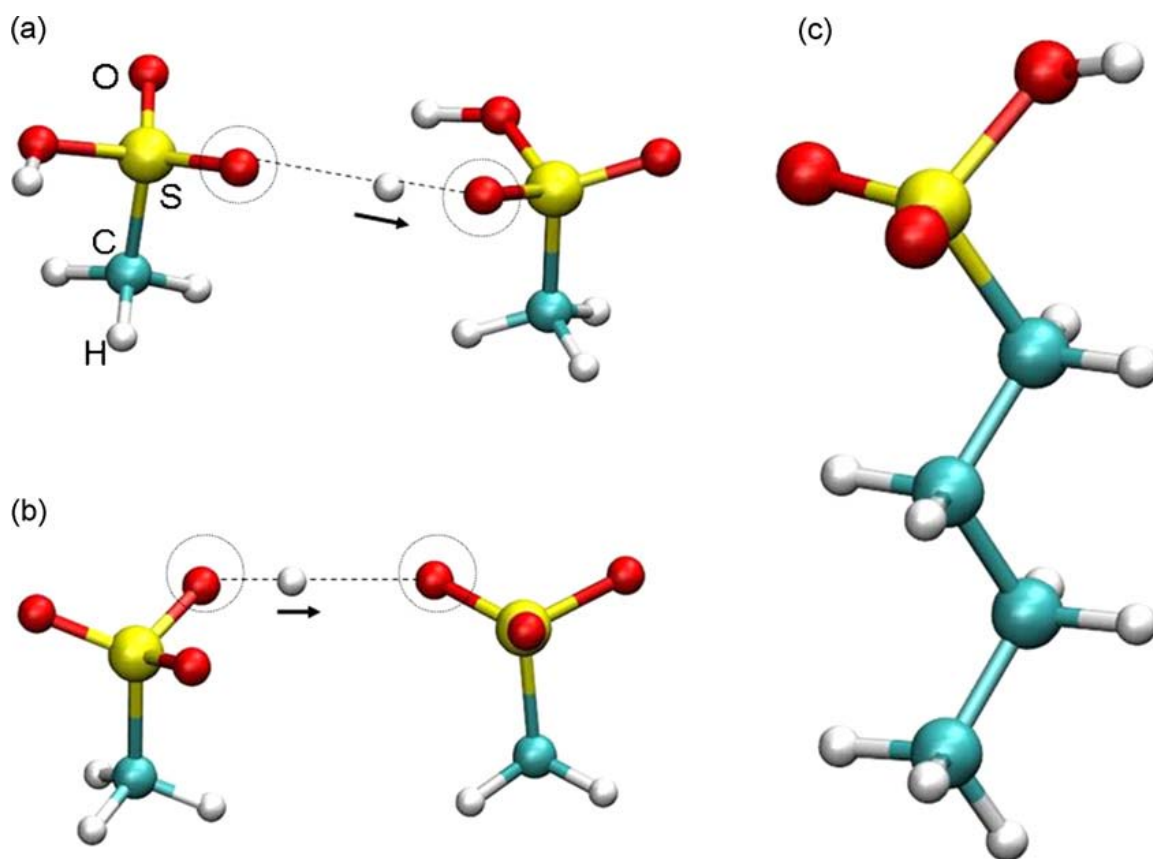


Figure 5. Modeling of the proton transfer in proton exchange membrane [8]

In the simplest picture, the proton transport is limited by the energy barrier the proton has to overcome. Usually, the barrier will be a function of the distance the proton has to bridge during hopping. The availability of SO₃H groups in the vicinity is also important. Only next neighbor groups are assumed to be involved in the transfer, so the proton exchange is always a pair interaction.

2.4. Sulfonated Polyimide Copolymer (SPI)

As illustrated before, many families of polymers with different chemical structures and various strategies for introducing sulfonic acid groups into the molecules have been explored as proton exchange membrane materials. Basically, there are two ways to obtain a new membrane: Pathway I is to modify the Nafion®-based membrane, using coating or blending methods to get a hybrid membrane. Pathway II is to synthesis it from the very beginning utilizing other polymeric monomers.

The research target is to use pathway II to synthesize a new membrane which can work at higher temperatures and have high performance/price ratio than Nafion®. According to the structure analysis of Nafion®, a conclusion comes into our sight: a polymer with mechanically and chemically stable back-bone and proton-exchanging end groups probably possesses the ability to act as a core part of the membrane electrode assembly (MEA). The target material is the sulfonated polyimide (SPI).

In this section, the advanced SPI proton exchange membranes for fuel cells developed in recent years will be introduced. From the progress in PEM area, the direction of development for the next generation materials for PEM applications will be revealed. The synthesis of polyimide materials that have attached ion conducting groups will be considered.

Polyimides are high temperature engineering materials characterized by cyclic structures that contain imide groups in the polymer chains, as shown in Figure 6.

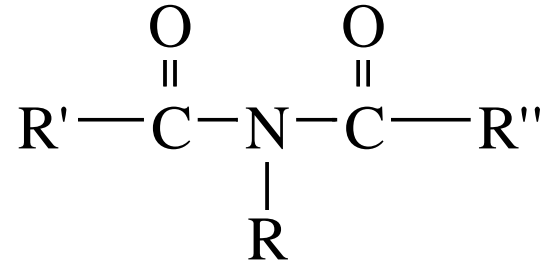


Figure 6. Chemical structure of polyimide

The first polyimide was produced in the early 1960s, but only in recent years has there been a rapid development for high strength composites, and thermally stable films, which have good resistance to temperature and dehydration, good mechanical performance and chemical stability. After sulfonation, it is believed to be a candidate with high potentials [9].

Basically, there are two kinds of polyimide: Five-membered ring one and six-membered ring one. Five-membered ring polyimides are high performance materials and have been investigated for many years.

Pineri and co-workers [10] synthesized five-membered and six-membered ring sulfonated polyimides from 4,4'-diaminobiphenyl-2,2'-disulfonic acid (BDSA), 4,4'-oxydianiline (ODA), and two types of dianhydrides, oxydiphthalic dianhydride (ODPA) and 1,4,5,8-naphthalenetetracarboxylic dianhydride (NTDA), respectively. In order to obtain a good compromise between the conductivity and hydrolysis stability, ion-exchange capacity (IEC) value was controlled. Membrane properties, such as swelling and conductivity [11], water vapor sorption and diffusion coefficients [12-14], and stability in aqueous medium [15], were studied and fuel cell performance based on a new design of the membrane electrode assembly (MEA)

[16] was tested. Their results showed that the sulfonated polyimide membranes had fairly good fuel cell performance while the proton conductivity was less than 0.01 S/cm at 100% relative humidity, which is a rather low value. And the ODPa-based sulfonated polyimides were not stable in fuel cell conditions, whereas NTDA-based sulfonated polyimides were relatively stable. Aromatic ether diamines were developed, which have different positions for amino-substituted or bulky groups in their structure, to help improve the hydrolysis stability and conductivity of the membranes. In the end, NTDA and BDSA were used to synthesize several series of SPIs to improve the hydrolysis stability and conductivity of the membranes. However, no better results had been achieved [17].

Based on the idea that bulky angled comonomers can push the polymer rigid rod backbone apart and produce nano-sized pores inside the membrane, Litt and co-workers [18, 19] have developed various random and sequenced SPIs by using BDSA, NTDA, and unsulfonated diamines with a bulky angled structure. Most membranes showed high conductivity (as high as Nafion® membranes at moderate relative humidity values and higher at high relative humidity levels) according to their report. However, these membranes had poor hydrolysis stability and poor mechanical strength, so no fuel cell testing data were reported.

A series of SPIs were prepared by McGrath and co-workers [20-22], using different sulfonated diamines, a commercially available sulfonated diamine, 2,5-diaminobenzene sulfonic acid (DABSA), and two self-synthesized sulfonated diamines, 3-sulfo-4,4'-bis(3-aminophenoxy) triphenyl phosphine oxide sodium salt (SBAPPO) and 3,3'-disulfonic acid-bis[4-(3-aminophenoxy) phenyl] sulfone (SA-DADPS). However, no conductivity and fuel cell performance data have been reported.

Intending to study structure–property relationship of SPIs systematically, Okamoto and co-workers [23-28] have developed two types of SPIs (main-chain type and side-chain type). They synthesized aromatic sulfonated diamines such as 4,4'-diaminodiphenyl ether-2,2'-disulfonic acid (ODADS) [24], 9,9'-bis(4-aminophenyl)fluorene-2,7-disulfonic acid (BAPFDS) [24], and 4,4'-bis(4-aminophenoxy)biphenyl-3,3'-disulfonic acid (BAPBDS) [25] and synthesized several series of main-chain type sulfonated polyimides by their copolymerization with NTDA and several common diamines. The obtained ODADS- and BAPFDS-based SPI membranes displayed higher proton conductivities and better hydrolysis stability than the corresponding BDSA-based ones. The BAPBDS-based SPIs showed greatly improved hydrolysis stability and similar or higher proton conductivities than Nafion® membranes. Although these membranes might be good candidates for low temperature (<80 °C) fuel cell systems, they might not have sufficiently good stability for high temperature applications (>80 °C) [24, 27].

To develop a micro-separated phase structure and ion-rich domain channels which are good for proton transport and similar to those in Nafion® membranes, Okamoto and his co-workers [25–27] also synthesized a novel type of side-chain SPIs using their self-developed sulfonated diamines, e.g., 2,2'-bis(3-sulfopropoxy)benzidine (2,2'-BSPB), 3,3'-bis(3-sulfopropoxy)benzidine (3,3'-BSPB), and 3-(2',4'-diaminophenoxy) propane sulfonic acid (DAPPS). Their results showed that the side-chain type SPIs, especially NTDA-2,2'-BSPB-based SPIs, had high proton conductivities of 0.2 S/cm at 80% RH and 105 °C and 0.05 S/cm at 50% RH and 120 °C. These SPIs might be expected to be good candidate membranes for high temperature PEM fuel cell applications; however, their thermal stability was not reported.

Shobha et al. [29] employed a novel sulfonated diamine containing a phosphine oxide moiety in the synthesis of a five-membered ring sulfonated polyimide. The synthesis is shown in Figure 7.

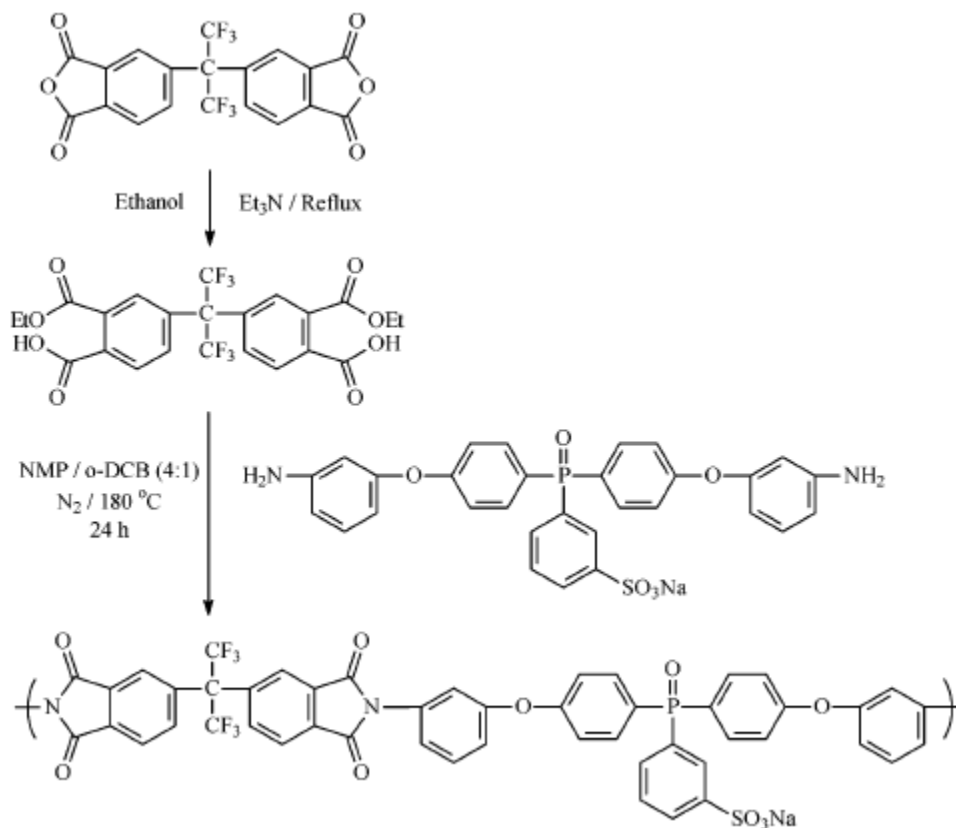


Figure 7. A five-membered ring sulfonated polyimide containing phosphine oxide [29]

However, when five-membered ring sulfonated polyimides are used for proton exchange membranes in fuel cells, they quickly degrade, while it has been realized that six-membered ring polyimides are much more stable in fuel cell environments than five-membered ring [30]. Probably hydrolysis of the five-membered ring imide structure leads to chain scission (decrease the molecular weight) and then causes the membrane to become brittle. Since the six-membered

ring polyimide is much more stable to hydrolysis, this chemical structure is in some degree better suited for PEM fuel cell applications but its stability is still questionable.

Genies et al has designed a synthetic method to produce random and block sulfonated copolyimides (SPIs) [31]. The first step in the synthesis is to prepare 4,4'-diamino-2,2'-biphenyl disulfonic acid (BDA) in short sequences and then it was condensed with 1,4,5,8-tetracarboxylic dianhydride (NDA), as shown in Figure 8. An adjusted ratio of these two monomers allows creating different block lengths of the sulfonated sequence. In the second polymerization step, the degree of sulfonation can be precisely controlled by adjusting the molar ratio of BDA and the unsulfonated diamine, which is 4,4'-oxydianiline (ODA) in SPI copolymer. It is critical to control the degree of sulfonation, because a high degree of sulfonation generally leads to high swelling or even dissolution of the polyimide membrane into water. It was also found three sulfonated repeat units in block length yield the highest proton conductivity [32].

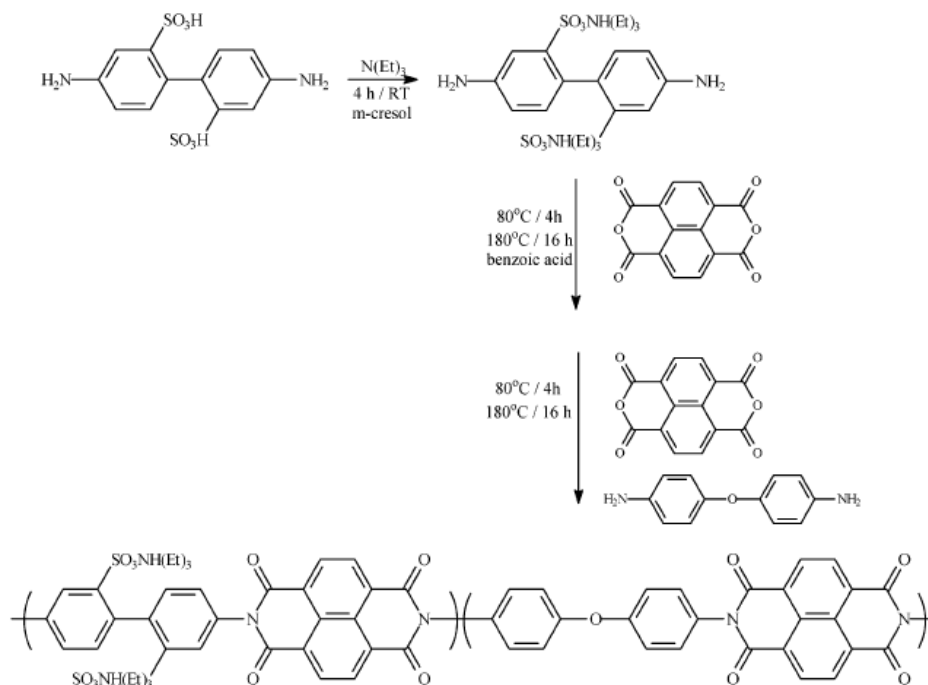


Figure 8. A sulfonated six-membered ring polyimide based on BDA, ODA, and NDA [32]

In this work, a random sulfonated polyimide with controlled sulfonation degrees was synthesized using commercially available sulfonated diamine, 4, 4'-diaminostilbene-2, 2'-disulfonic acid (DSDSA), NTDA, and other common diamines. The physical properties and proton conductivities of the membranes were investigated, and their potential application for high temperature PEM fuel cells was explored.

2.5. Membrane Electrode Assembly (MEA)

Just like the heart for human body, the membrane electrode assembly (MEA) is like the proton exchange membrane fuel cell's heart. A membrane electrode assembly is an assembled stack of proton exchange membrane (PEM), catalyst and flat plate electrodes (Figure 9).

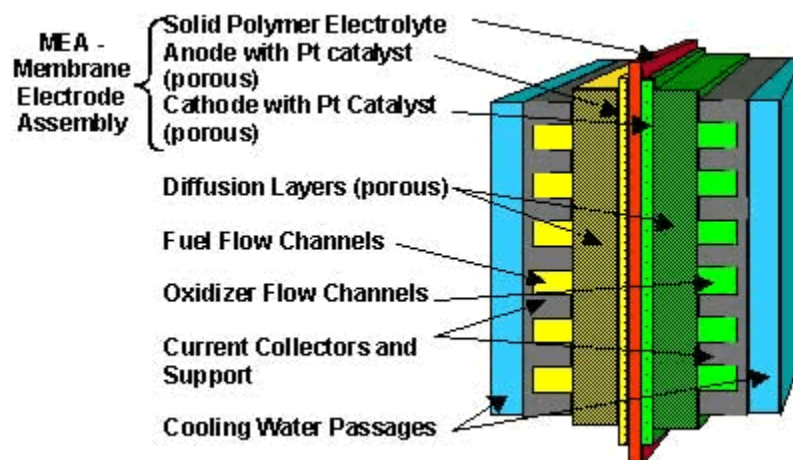


Figure 9. Main components of PEMFC [33]

In PEMFCs, the MEAs are connected with bipolar plates. The solid proton exchange membrane can not diffuse into the porous electrode structures. The electrolyte-gas interface has two dimensions, so there might be parts that do not adhere to each other. As a result, a special

bonding (gasket seal) is used to obtain a high interface area between the membrane and electrode assemblies.

To provide sufficient catalytic activity, platinum or its alloy is applied to the MEA. That is one of the main reasons for the high price of the PEMFCs. Catalyst layer can be applied directly to the membrane by many different methods. Metallic catalyst can be formed on the proton exchange membrane side, or on the gas diffusion layer and attach to the PEM.

There are normally three ways to increase the performance of the MEA:

- To accelerate the chemical reaction by increasing the concentration of the catalyst.
- To increase the temperature surrounding it, but too high temperature may break the PEM.
- To increase the electrode area, which is one common way for stationary applications, but not good for mobile use.

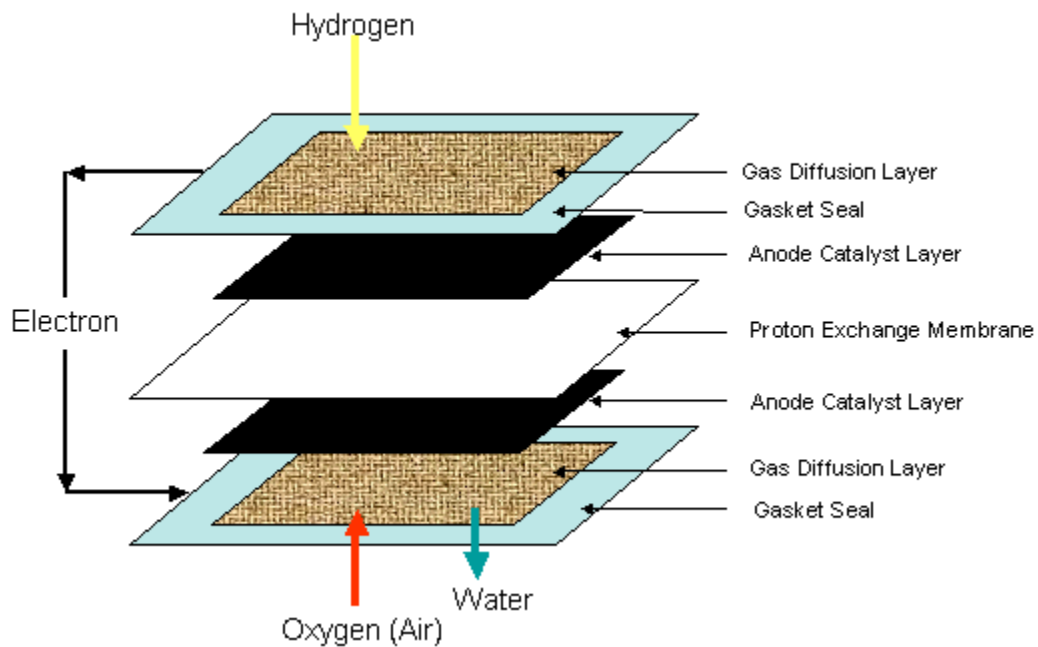


Figure 10. Main components of MEA [34]

There are three major parts of the MEA (Figure 10): catalyst layer, electrode layer and gas diffusion layer. The electrode layer can also be considered as the proton exchange membrane, the catalyst layer and gas diffusion layer will be introduced briefly.

2.6. Catalyst Layer (CL)

Platinum based catalyst is the most suitable for the MEA in PEMFC applications; however, the price is an issue for commercial application (Figure 11). Therefore, instead of pure platinum, small alloy particles are deposited finely onto the carbon particles to form low price catalyst [34].

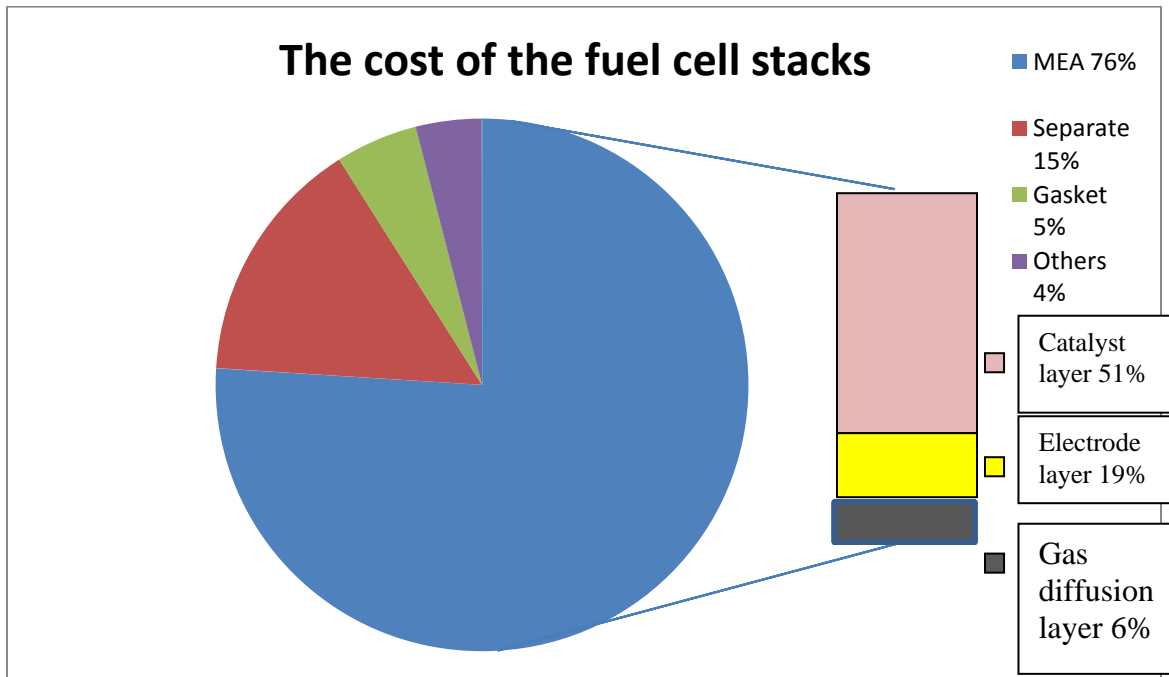


Figure 11. Cost of fuel cell stack in 2008 [34]

2.7. Gas Diffusion Layer (GDL)

The gas diffusion layers in the PEMFC are usually made of a porous paper or cloth; the thickness is typically 0.3-1.0 mm. The gas diffusion layers are attached to the bipolar plates on both anode and cathode side.

There are four main functions of the gas diffusion layers in the MEAs:

- To provide the reactant gases (oxygen and hydrogen) with even distribution from flow field channels to catalyst layer,
- To conduct the electrons to the electron collectors,
- To provide passage for removal of water from the catalyst layer to flow field channels,
- To support the thin, brittle PEM and catalyst layer against the compressive forces.

Chapter Three

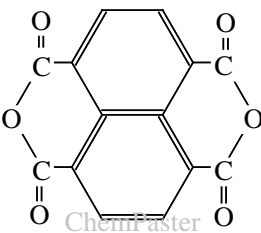
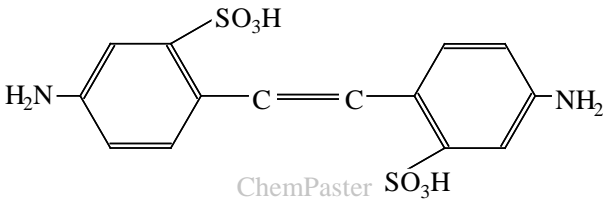
Manufacturing and Characterization of SPI Copolymer Based Proton Exchange Membrane

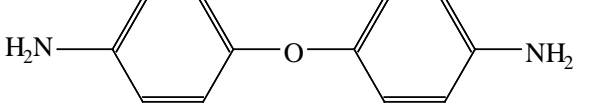
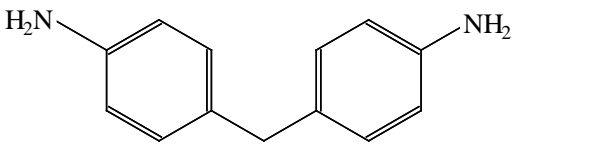
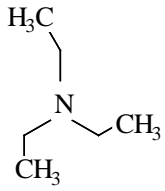
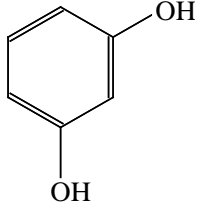
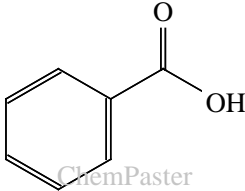
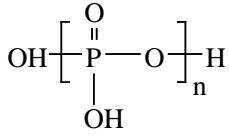
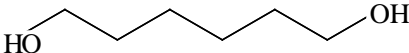
This section describes manufacturing and characterization of the SPI copolymer in detail.

3.1. Materials Used

The materials used to produce the SPI based membrane are listed in Table 1. NTDA, DSDSA, MDA and ODA were dried in a vacuum oven at 120° C overnight.

Table 1. Materials used to produce the SPI based membrane

Chemical Name	Chemical Structure
1,4,5,8-Naphthalenetetracarboxylic Acid (NTDA)	
4,4'-Diaminostilbene-2,2'-disulfonic Acid (DSDSA)	

4,4'-Diaminodiphenyl Ether (ODA)	
4,4'-Diaminodiphenylmethane (MDA)	
Triethylamine	
3-Methylphenol (m-cresol)	
Benzoic Acid	
polyphosphoric acid (PPA)	
1,6-hexanediol	

3.2. Synthesis of DSDSA-based SPI Copolymers

First, 2.5g (7.0mmol) DSDSA, 50ml m-Cresol and 1.7g triethylamine were added into 250ml, 4-neck flask with stirring device. The mixture was heated at 80°C in N₂ atmosphere until DSDSA was completely dissolved. Then, 0.6g (3.0mmol) ODA, 2.6g (10.0 mmol) NTDA, and benzoic acid were added successively followed by the addition of 15ml m-Cresol. The mixture was stirred at 80°C for 4 hours, at 180°C for 16 hours and at 200°C for 4 hours. After cooling to the room temperature, 50 ml m-Cresol was added. The solution was precipitated into excess isopropyl alcohol (IPA) to filter and wash. Finally, fiber-like copolymer was collected in the vacuum oven overnight.

As a result, as shown in Figure 12, SPI polymers with different ratios of blocks were synthesized through polycondensation of the following monomers: 1,4,5,8-Naphthalenetetracarboxylic acid (NTDA), 4,4'-Diaminostilbene-2,2'-disulfonic acid (DSDSA) and 4,4'-Diaminodiphenyl ether (ODA) or 4,4'-Diaminodiphenylmethane (MDA). In this reaction, “one step” high temperature copolymerization was carried out in m-cresol in the presence of triethylamine and benzoic acid. This method has been extensively employed in the literature [20, 22–24]. The monomer NTDA was kept as (x+y) mol, which was the total amount of DSDSA and ODA or MDA. The degree of sulfonation was controlled by adjusting the ratio of DSDSA. A higher ratio of DSDSA in the copolymer should result in higher proton conductivity; however, as DSDSA's ratio increases, the mechanical and thermal properties probably decrease due to the increasing flexible C=C double bonds.

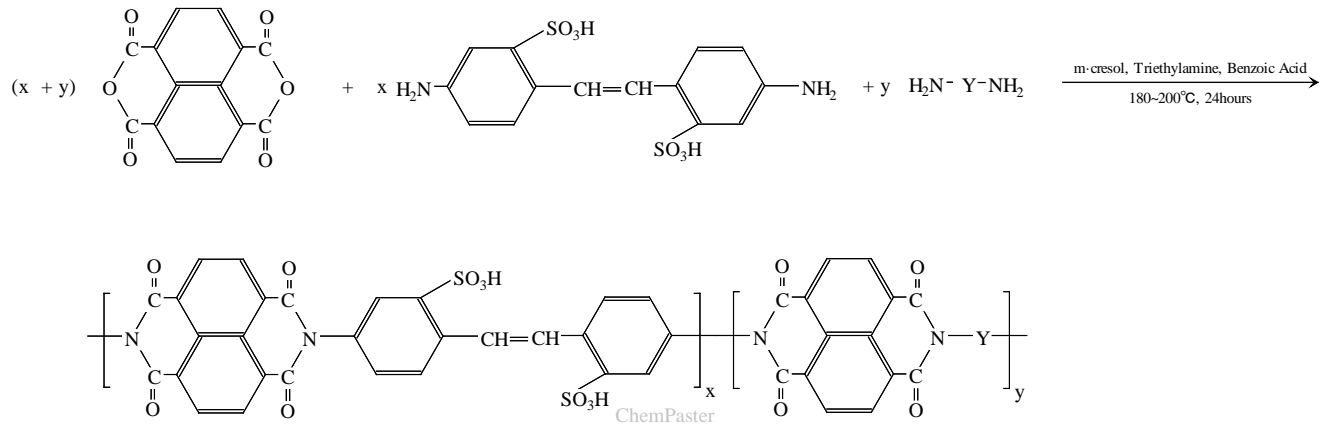


Figure 12. Chemical reaction for synthesis of SPI

3.3. Membrane Manufacturing

The copolymer was dissolved in m-Cresol. The membrane was formed by casting the solution onto a clean glass dish and drying at 90°C for 12 hours. Using a razor blade, the membrane was collected after it cooled down to the room temperature. The film was soaked in methanol at 60°C for 1 hour to clean the surface. The film was immersed in 1.5mol/L HCL at room temperature for 48 hours for doping. Finally, the membrane was washed by deionized water and dried in vacuum oven at 120°C overnight (Figure 13).

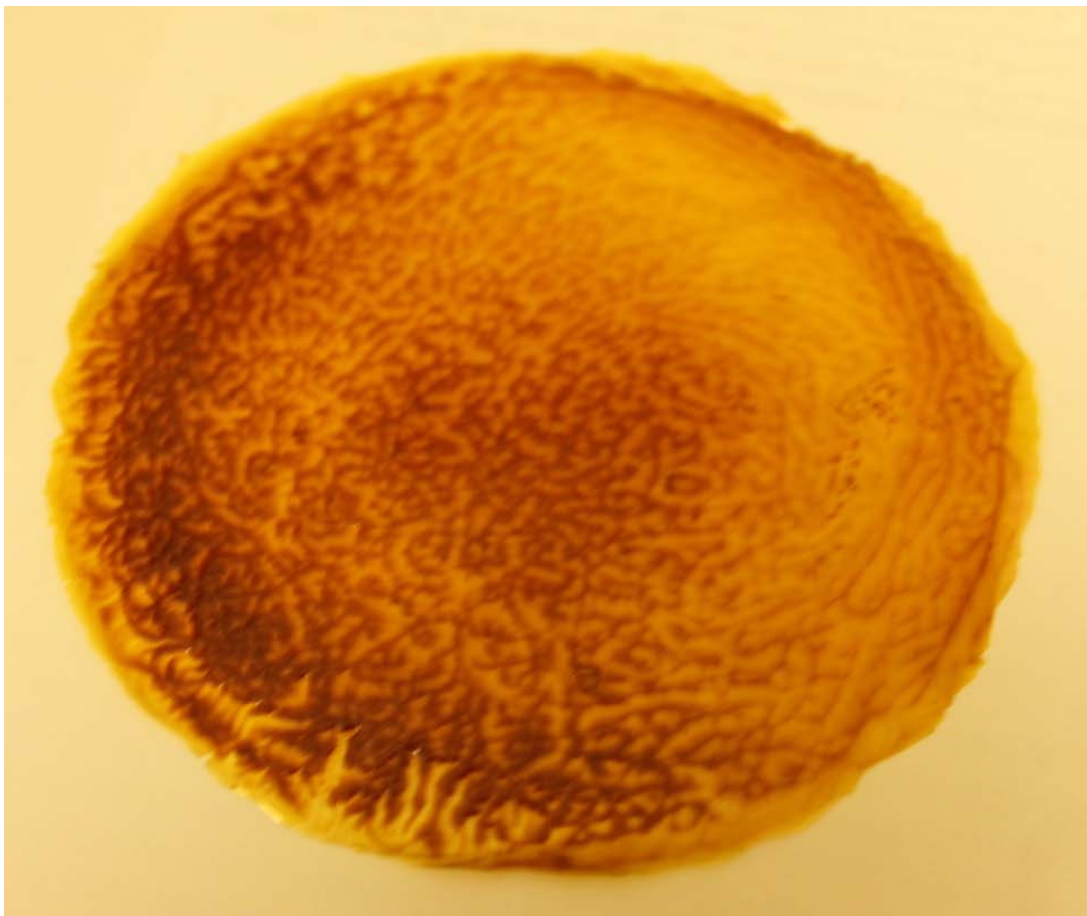


Figure 13. SPI copolymer membrane

3.4. Polymer and Membrane Characterization

The Fourier transform infrared (FT-IR) measurements were performed on a Nicolet 6700 FT-IR spectrometer of Thermofisher Scientific (Figure 14). Differential Scanning Calorimetry (DSC) measurements were carried out on a DSC Q2000 TA instrument (Figure 15).

Thermogravimetric (TGA) curves were obtained on a TGA Q500 instrument (Figure 16) at a heating rate of 15 °C/min in N₂ flow. Water uptake was calculated according to the ASTM D 570-98. Ion exchange capacity (IEC) and proton conductivity of the membrane were measured.

The mechanical tests were performed in an Instron machine including the tensile and the tear tests (Figure 17).



Figure 14. Nicolet 6700 FT-IR spectrometer

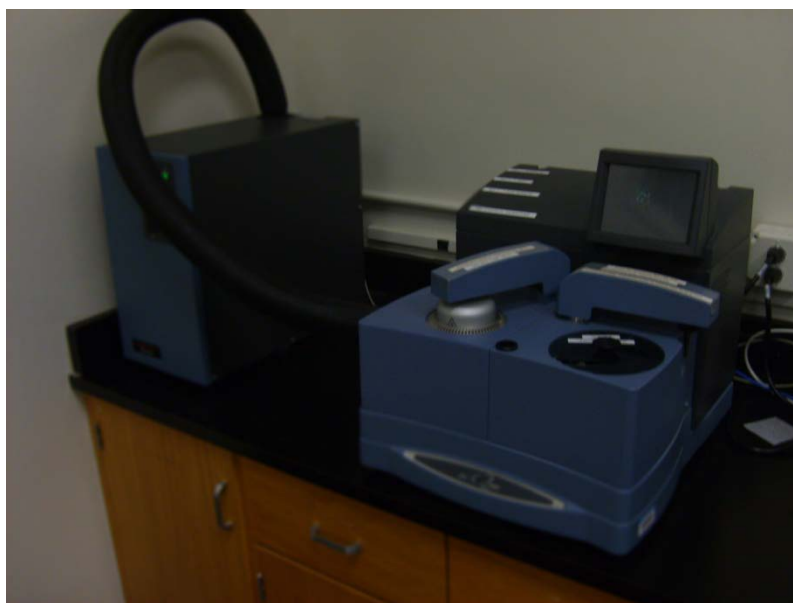


Figure 15. DSC Q2000 TA instrument

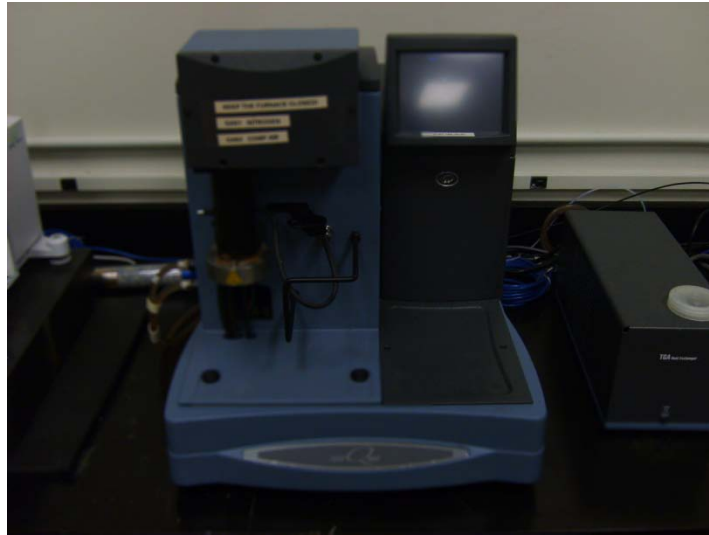


Figure 16. TGA Q500 instrument



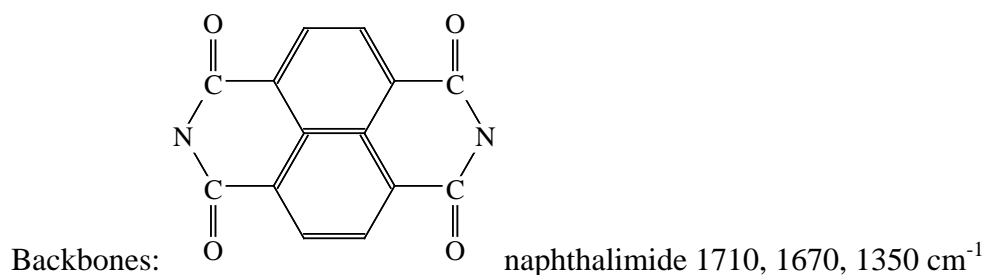
Figure 17. Instron machine

3.4.1. FTIR Analysis

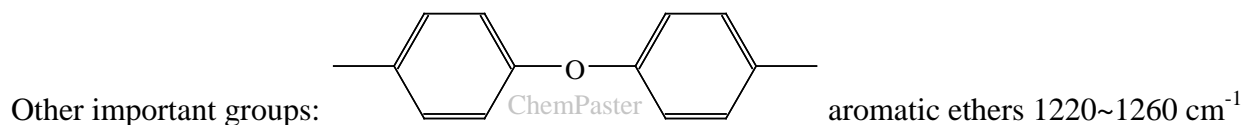
Tough, ductile membranes were obtained by dissolution of the copolymers in their salt forms in m-cresol and subsequent solution casting onto clean glass plates. The membranes were treated and acidified using the methods described earlier.

The completion of proton exchange was confirmed by IR spectrum and IEC measurements. FTIR spectrum testing was performed for the characterization of element and bonding of the SPI membrane. Figure 18 shows the FTIR spectrum of the NTDA-DSDSA/OD copolymer. It displays the naphthalimide absorption bands at 1710, 1670, and 1350 cm^{-1} , respectively. The broad bands at 1020 and 1080 cm^{-1} are assigned to the symmetric and asymmetric stretches of the sulfonic acid groups.

This spectrum exhibited a series of SPI's distinctive absorption peaks:



Side group: $-\text{SO}_3\text{H}$ sulfonic acid group 1020, 1080 cm^{-1}



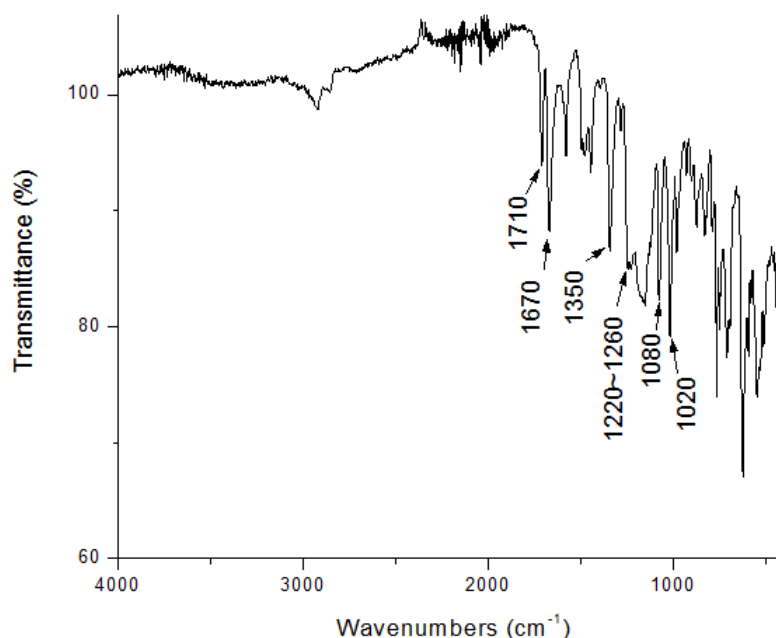


Figure 18. FTIR testing of the ODA based diamine SPI membrane

From the FTIR data, ODA based diamine SPI based copolymer is confirmed to be synthesized successfully.

3.4.2. Thermogravimetric Analysis (TGA)

The TGA testing was performed at N₂ atmosphere; the temperature increased from room temperature (25°C) to 800 °C at a rate of 15°C/min.

Figure 19 shows the TGA curves of the SPI copolymer. It was obvious that the SPI had three steps thermal degradation pattern. Initial weight loss of the SPI based membrane occurs before 137.77°C, which is mainly due to the evaporation of the absorbed water in the membrane. The second weight loss was observed around 380-400°C which is mainly associated with the elimination of the sulfonate groups. The third weight loss step was around 530-550 °C, which

corresponds to the pyrolysis of the backbone of the SPI copolymer. This may be caused by the thermal degradation of sulfonate groups at relatively low temperatures compared to the polymer backbone. The SPI copolymer based membrane still had 80% weight remaining at 325°C. The TGA curves clearly indicate that the SPI copolymer has remarkable thermal stability, which makes it suitable for relatively high temperature fuel cell operating conditions. The DSDSA-based copolymers have a similar thermal stability to those of the other types of SPIs published in the literature [23].

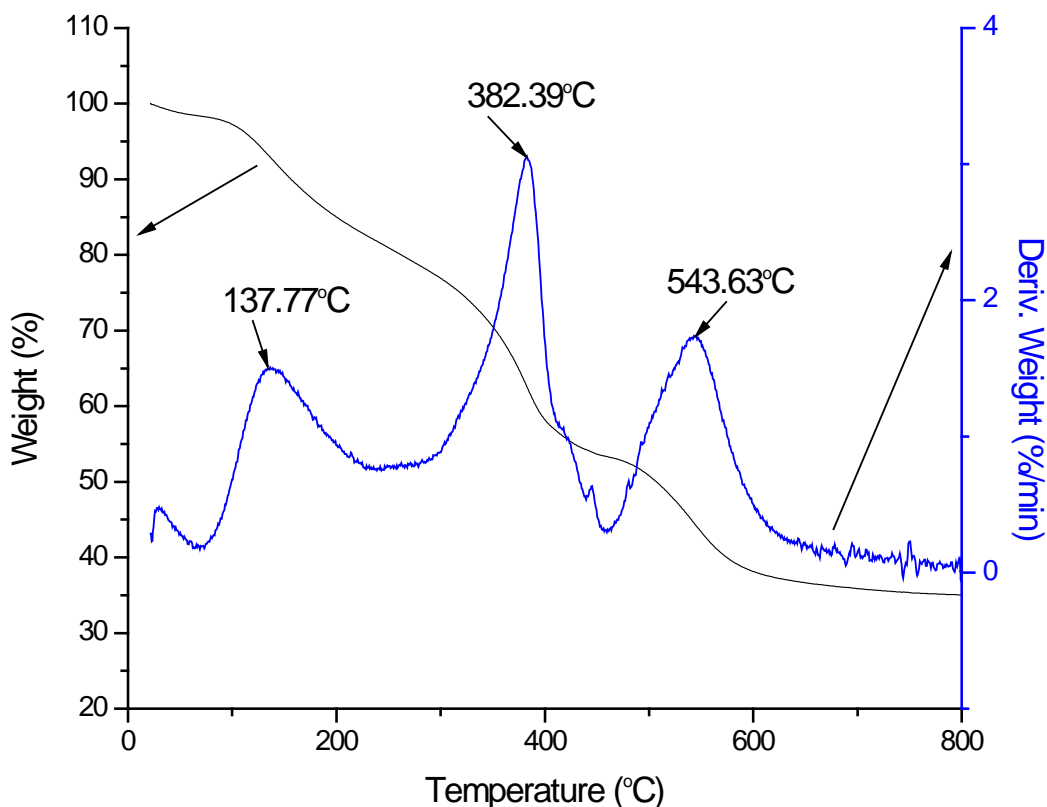


Figure 19. TGA testing of the SPI membrane

3.4.3. Differential Scanning Calorimetry (DSC)

The SPI copolymer based membranes were cut into small pieces as testing samples with a weight of 1.15mg.

Testing procedure:

- ramp from room temperature (25°C) to 350°C (rate 15°C/min)
- isothermal for 15 minutes.
- ramp from 350°C to 25°C (rate 15°C/min)
- isothermal for 15 minutes
- ramp from room temperature to 350°C (rate 15°C/min)

From Figure 20, the crystallization temperature is 193.33°C and the glass transition temperature is 74.27°C. There is no obvious melting temperature but it is likely to be 212.13°C. This is mainly due to the SPI copolymer's low crystallinity and high amorphous regions, which is like thermosets' performance, having order over short distances but not over longer distances. It can be seen that the SPI has a higher glass transition temperature (T_g) than pure polyimide. This is probably because the introduction of sulfonate groups may have two kinds of effects on T_g of the polyimide: one is to increase the intermolecular interaction by pendant ions, i.e. ionomer effect; the other is to increase the molecular bulkiness. Both effects hinder internal rotation, which further leads to the increase of the glass transition temperature.

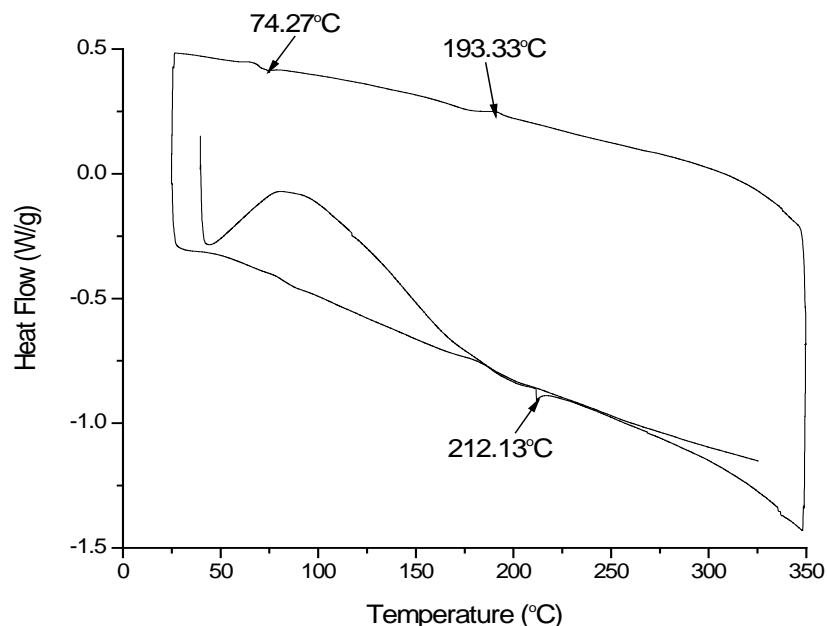


Figure 20. DSC testing of the SPI membrane

3.4.4. Water Uptake

The proton conductivity and mechanical stability of PEMs are strongly related to the presence of water. The proton exchange reaction requires a large amount of water to coordinate with protons as they move through the membrane. Generally speaking, proton conductivity depends on the number of available acid groups and their dissociation capability in water, which is accompanied by the generation of protons. Water molecules lead to dissociation of the acid functional groups and help proton transport; therefore the water uptake is an important parameter in studying PEM membranes. However, excessive water uptake will lead to the loss of mechanical strength, which will limit the practical application of the membrane in fuel cells.

Water uptake values of the SPI copolymer membranes were determined according to the ASTM D 570-98 (2010) e1- standard test method for water absorption of plastics. One piece of

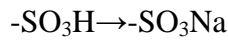
the SPI membrane was prepared using the following steps: membrane was heated at 105 °C for 1 h and then at 50 °C for 24 h in an oven; then, the membrane was cooled down to room temperature, weighed immediately and then soaked in deionized water at room temperature for 24 h. The membrane was removed, gently wiped with tissue paper, and weighed again [35-41]. The water uptake value was calculated as follows:

The weight of fully dried membrane (W_{dry}) was 0.0805g; after soaking, the weight (W_{wet}) became 0.1083g.

$$\text{Therefore, the water uptake WU(\%)} = \frac{W_{wet} - W_{dry}}{W_{dry}} \times 100 = 34.53\%$$

3.4.5. Ion Exchange Capacity (IEC)

The IEC of the membrane plays a crucial role in evaluating the water uptake and proton conductivity. The IEC of the SPI membrane was measured by the titration method. First, 0.1~0.2g dried membrane sample was immersed in 1.0M saturated NaCl solution at 50°C for 48 hours to free the H⁺ ions (the H⁺ ions in the membrane were replaced by Na⁺ ions).



Then the H⁺ ions released from the membrane were titrated with 0.01M (C_{NaOH}) NaOH using bromophenol blue as indicator. The titrated IEC of the membrane was determined by:

$$\text{IEC} = \frac{C_{NaOH} V_{NaOH}}{W_p}$$

where V_{NaOH} is the titrated volume of NaOH, C_{NaOH} is the concentration of the NaOH and W_p is the weight of the dried membrane.

The weight of the dried membrane (W_p) is about 0.1789g and the NaOH used in the titration (V_{NaOH}) is 22.4 cm⁻³, so the IEC obtained according to the equation is 1.25mmol/g. For

comparison, the IEC of Nafion®117 membrane is 0.909 mmol/g at the same temperature (30°C) as reported in the literature [42].

3.4.6. Proton Conductivity Measurement

A container was filled with ammonia water and its pH was measured (Figure 21). A parafilm was attached to the bottom of a tube and sealed. To make sure it was sealed, some water was added to the tube. Using a 9V battery as the power source, it was observed that there was no change in the pH level of the ammonia water.

The parafilm was replaced with the membrane whose proton conductivity will be measured (SPI membrane in this case). Immediately, it was observed that the pH of the ammonia water dropped, and there were a lot of small bubbles produced around the copper wire in the ammonia water. This phenomenon proves that protons can pass through the SPI membrane to react with the OH⁻.

The reaction in the anode: $2\text{Cl}^- \rightarrow \text{Cl}_2 + e^-$

The reaction in the cathode: $2\text{NH}_4^+ + 2e^- \rightarrow 2\text{NH}_3 + \text{H}_2$

The reaction under the membrane $\text{H}^+ + \text{OH}^- \rightarrow \text{H}_2\text{O}$

The overall reaction $2\text{HCl} + 2\text{NH}_4\text{OH} \rightarrow \text{Cl}_2 + 2\text{NH}_3 + \text{H}_2 + \text{H}_2\text{O}$

The cross-sectional area of the membrane in the tube and the change in the pH level can be measured to calculate the proton conductivity. Different types of proton exchange membranes can be tested and compared with this new method.

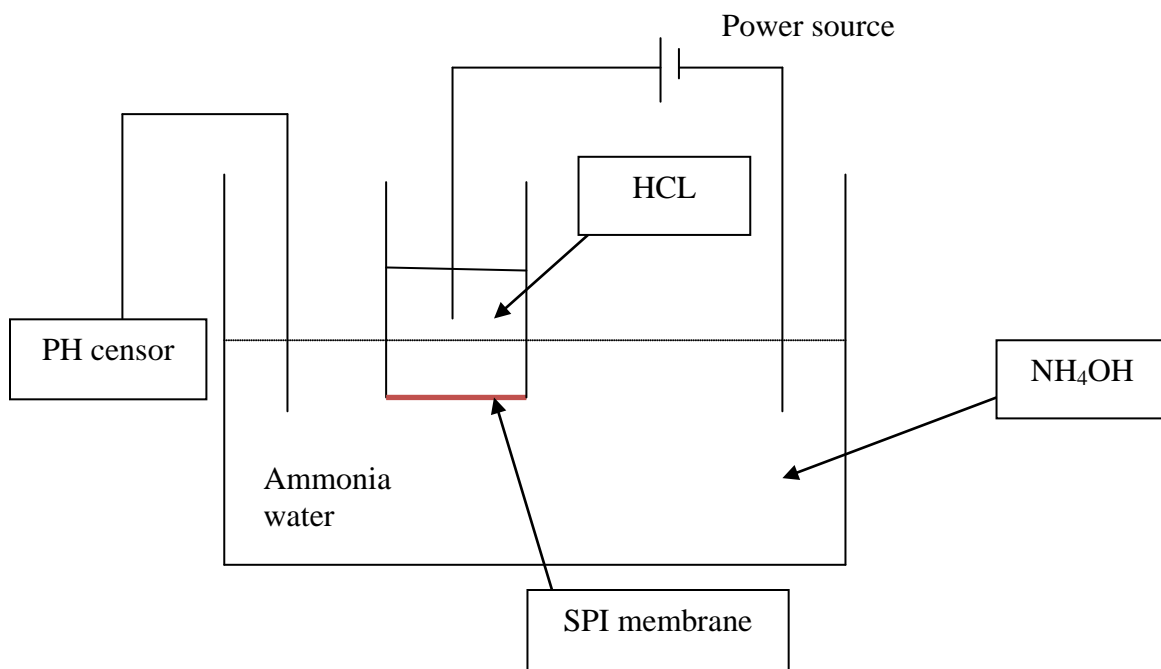


Figure 21. Schematic of the membrane proton conductivity measurement

The proton conductivity of the membrane was determined by:

$$\sigma = L / (A \times R)$$

where the σ is the proton conductivity, L is the thickness of the membrane, A is the cross sectional area of the membrane perpendicular to the flow and R is the measured resistance.

The thickness (L) of SPI membrane is around 150 micron, cross sectional area (A) is 0.125 cm², resistance (R) is 10 Ω . Therefore, the calculated proton conductivity of the SPI membrane is around 0.012S/cm, while the conductivity of Nafion® reported in the literature is around 0.1 S/cm at 100% RH and 30 °C [43].

3.4.7. Mechanical Tests

Novel membranes must also be adaptable and have the necessary physical strength and ductility in dry and wet states to survive the stress of electrode attachment. Proton exchange membranes with good mechanical properties in both dry and hydrated states are critical to successful MEA fabrication and long-term durability in a fuel cell device.

The mechanical tests consist of two parts: tensile tests and tear tests.

The tensile test was done according to ASTM D882-02 method – standard test method for tensile properties of thin plastic sheeting.

Before the tensile test, the SPI membranes with different thickness were cut into small rectangles (3 cm in length and 0.9 cm in width). And then were put on an Instron machine for tensile testing at 50%RH and 23°C. Table 2 shows the final testing data:

Table 2. Raw data of the SPI membrane tensile tests

	Thickness (mm)	Elongation at Maximum Load (%)	Maximum Load (N)	Tensile stress at Maximum Load (MPa)	Modulus (E-modulus) (MPa)
1	0.060	10.3	9.5	17.6	602.0
2	0.080	11.2	18.2	25.3	564.9
3	0.030	14.0	14.0	51.7	1033.6
4	0.060	17.9	18.9	34.9	695.2
5	0.020	10.9	9.1	50.4	1088.2
Mean	0.050	12.8	13.9	36.0	796.8
CV%	49.0	24.6	33.3	41.9	30.9

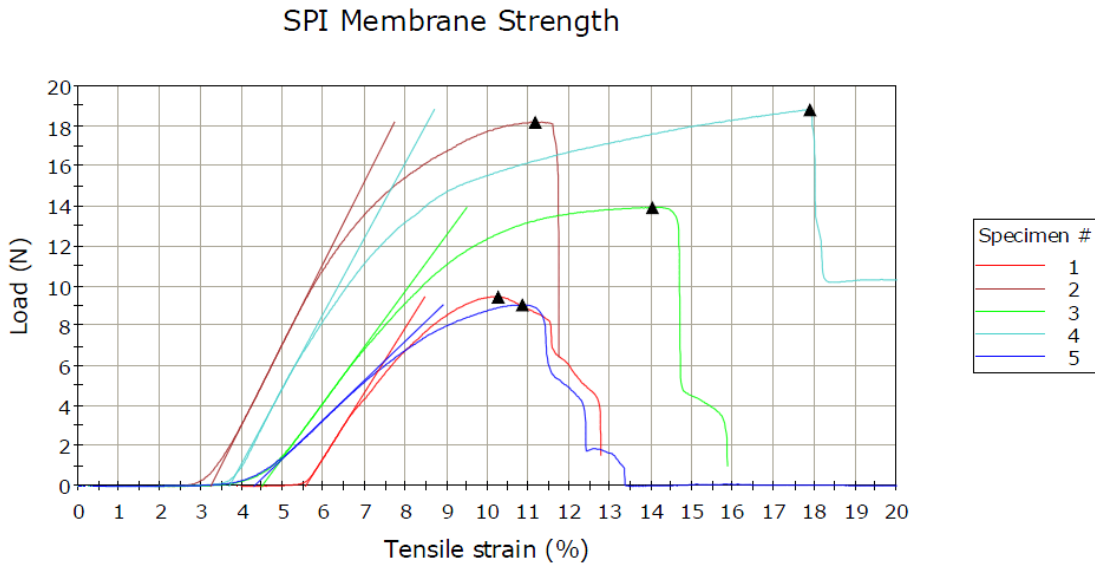


Figure 22. Load versus tensile strain curves of the SPI membrane samples

Figure 22 shows the tensile load-strain behavior of the SPI membranes with different thicknesses. Generally speaking, the SPI is very brittle, and the maximum load values decreased with the SPI membrane's thickness decreases for all samples except Sample 1. This is probably because Sample 1 has some interfacial debonding and incoherence due to non-smooth surface. Tensile stress at maximum load increased with the SPI membrane's decreasing thickness. Compared with the data of Nafion®, the SPI membrane's modulus is much higher (796.8MPa versus 294 MPa of Nafion®), possibly indicating that SPI membrane is more brittle than Nafion®, however, the tensile strength of SPI membrane is very close to that of Nafion® (30 MPa versus 32MPa in TD). The data related to Nafion® is concluded in table 3.

Table 3. Data for Nafion® tensile test [44]

Property	Typical Value	Test Method
Physical Properties		
Tensile Modulus, MPa (kpsi)		
50% RH, 23 °C	249 (36)	ASTM D 882
water soaked, 23 °C	114 (16)	ASTM D 882
water soaked, 100 °C	64 (9.4)	ASTM D 882
Tensile Strength, maximum, MPa (kpsi)		
50% RH, 23 °C	43 (6.2) in MD, 32 (4.6) in TD	ASTM D 882
water soaked, 23 °C	34 (4.9) in MD, 26 (3.8) in TD	ASTM D 882
water soaked, 100 °C	25 (3.6) in MD, 24 (3.5) in TD	ASTM D 882
Elongation at Break, %		
50% RH, 23 °C	225 in MD, 310 in TD	ASTM D 882
water soaked, 23 °C	200 in MD, 275 in TD	ASTM D 882
water soaked, 100 °C	180 in MD, 240 in TD	ASTM D 882

The tear test was done according to the ASTM D1938-06 method – standard test method for tear- propagation resistance (trouser tear) of plastic film and thin sheeting by a single tear method.

Before the tear test, the SPI membranes with different thicknesses were cut into small rectangles (3.81 cm in length and 1.27 cm in width), and then were cut a slit according to Figure 23. After that, the sample was put on the Instron machine for tear testing in 50% RH and 23°C. According to Table 4, the SPI membrane is so sensitive that only can stand 11.05 cN tearing force at the highest level, then it breaks; this is one of the biggest problems that the proton exchange membranes have. So cautions must to be paid that the membrane is vulnerable to the tearing when the SPI membrane is used into the commercial application, the special protection must be added to keep it from bending to tear.

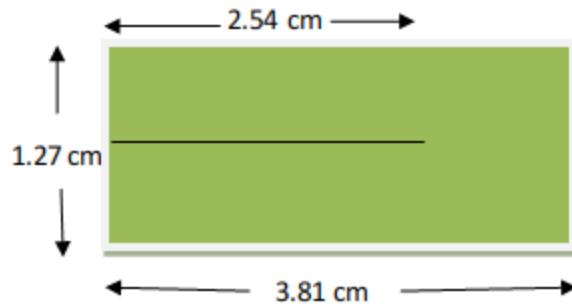


Figure 23. Dimensions of SPI membrane sample for tearing test

Table 4. SPI membranes tear test data

	Maximum Load (cN)	Extension at Maximum Load (mm)	Average Tearing Load (Integral) (cN)
X 1	10.49	27.94	0.37
2	5.48	24.55	1.82
3	5.65	2.54	1.69
4	25.24	15.66	5.34
5	7.85	10.58	3.14
Mean	11.05	13.34	3.00
CV%	86.10	69.19	56.39

Chapter Four

Manufacturing of the SPI Membrane Based Membrane Electrode Assembly and Testing the Fuel Cell

This section describes manufacturing and assembly of the MEA of PEM fuel cell and its testing.

4.1. Preparation of the MEA

After the characterization of the SPI membrane, the next step was to use it in a fuel cell for testing; therefore, an MEA was made with the following steps:

- Two carbon fabrics were cut into a square shape (7.1cm×7.1cm)
- Ammonium ferric oxalate (AFO) solution preparation. A dark room was used for this purpose such that AFO would not transform into another matter under light. First, 0.55ml water and 0.3g AFO were weighed and mixed into a solution which was stored in a cool, dark room for 24 hours.
- Platinum (Pt) solution preparation. 0.2g tetrachloroplatinate and 0.39ml warm water were mixed together in a water bath at 47°C.
- The AFO solution prepared earlier was mixed with the Pt solution immediately at about 38°C.

- The carbon fabrics were coated with the mixed solution evenly.
- Finally, the SPI membrane and coated carbon fabrics were assembled into a sandwich construction (Figure 24); two aluminum sheets were used as frame to temporarily seal the edges.

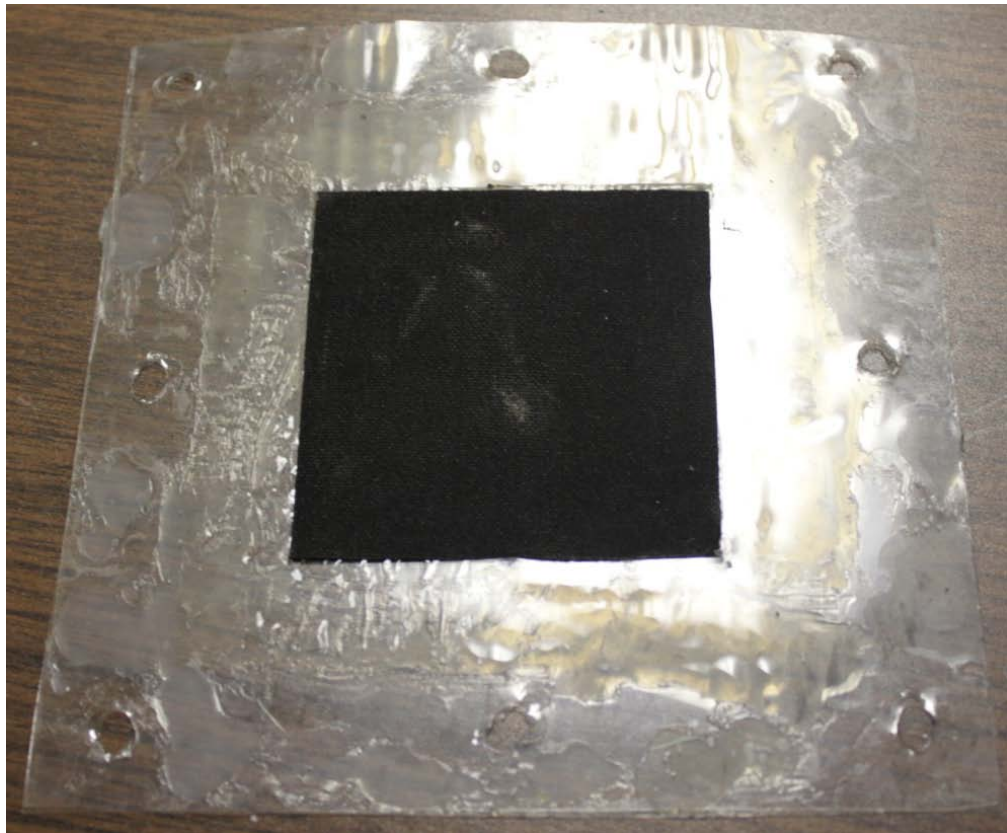


Figure 24. SPI membrane based MEA

4.2. Assembly of the Fuel Cell

The fuel cell was assembled using the MEA, two graphite plates with different runners and two PVC end plates with Nickel current collectors.

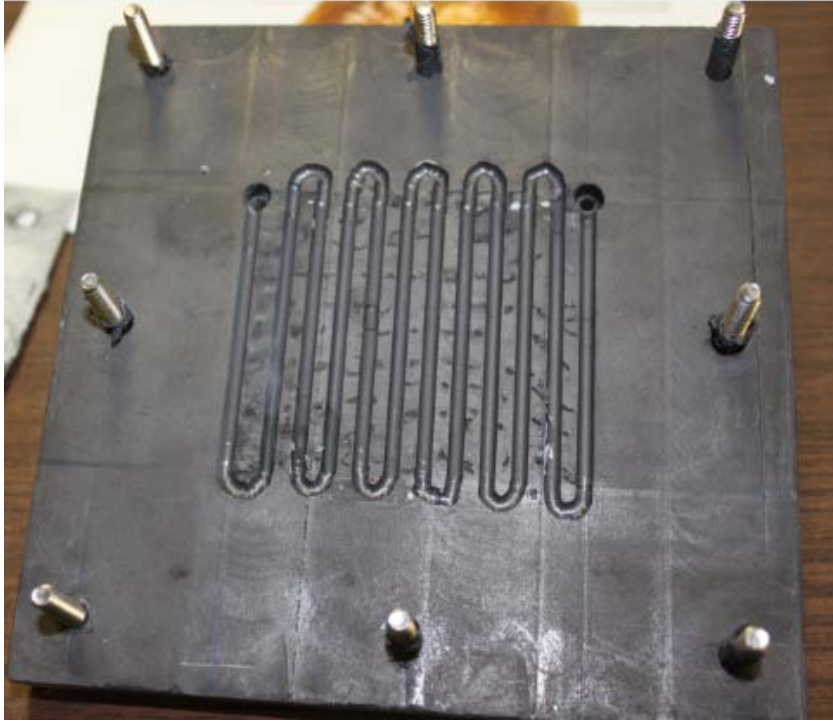


Figure 25. Graphite plate with U-shape runner [45]



Figure 26. Graphite plate with linear runner [45]



Figure 27. PVC end plate with Nickel current collector [45]

The graphite plate for the hydrogen side had a U-shape runner to make sure the hydrogen reacts completely in the channel. Linear runner was used for the air side to allow more air passage (Figure 25 and 26). After assembling, the fuel cell was tested using a digital multimeter at different hydrogen flow rates.

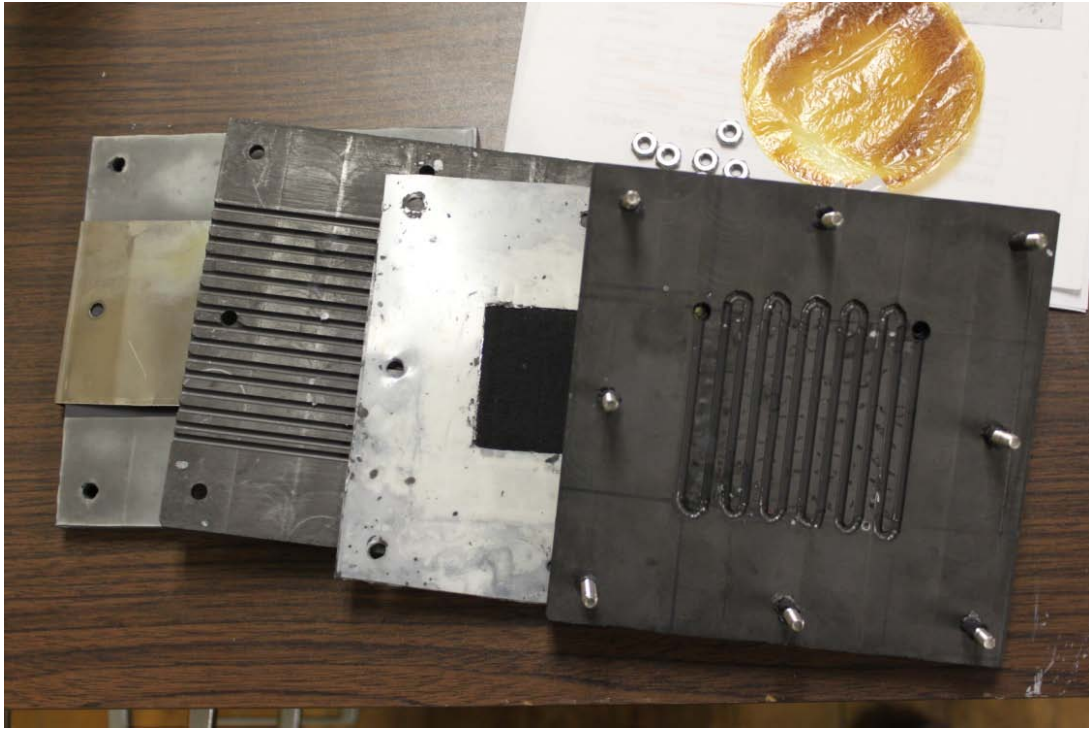


Figure 28. Components of the fuel cell before assembling [45]

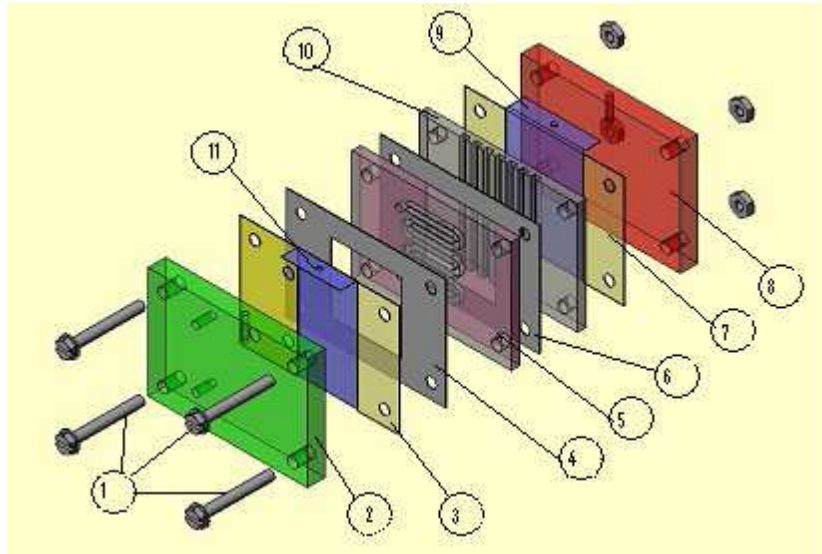


Figure 29. Schematic of the manufactured PEMFC [45]

Before the fuel cell was assembled, all the parts had to be cleaned, which are shown in Figure 28. The components of the air/hydrogen proton exchange membrane fuel cell are shown in Figure 29. The components are: 1-assembly bolts, 2-hydrogen side end plate, 3-silicon rubber strip gasket, 4-silicon rubber gasket, 5-hydrogen flow field plate 6-MEA and Mylar gaskets 7-Silicon rubber strip gaskets, 8-air side end plate, 9-air side metal electrode, 10-air flow field plate and 11-hydrogen side metal electrode. Cell compression is achieved by tightening the eight shoulder screws that squeeze against aluminum end plates. Maintaining even pressure over the cell is important to prevent leaks that might decrease the cell performance. In order to achieve even pressure, the screws were cross tightened by hand.

4.3. Fuel Cell Testing

The single air/hydrogen PEMFC containing the SPI membrane was tested (Figure 30). A standard flow meter was attached between the hydrogen tank and the fuel cell using plastic pipes, and a voltage meter was attached between the anode and cathode of the fuel cell. When the valve of the hydrogen tank was opened, the hydrogen flow rate was recorded immediately, and measuring the cell voltage was done using a model MV 110 digital voltmeter. The voltage values were read from the voltmeter under the same conditions in every 5 seconds. Several tests were performed under different flow rates. The fuel cell voltage variation at 3.45ml/min hydrogen flow rate, 1ATM and 25°C is shown in Figure 31. The hydrogen purity was 99.99%.

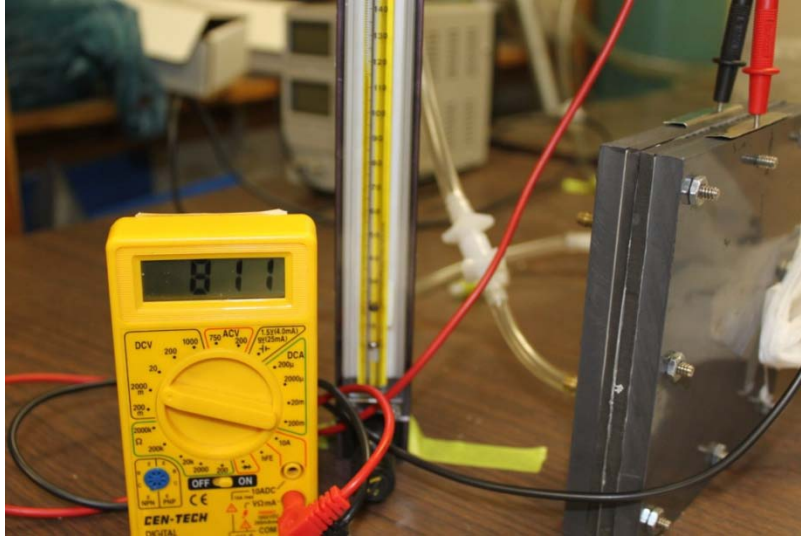


Figure 30. Testing of the SPI membrane based fuel cell

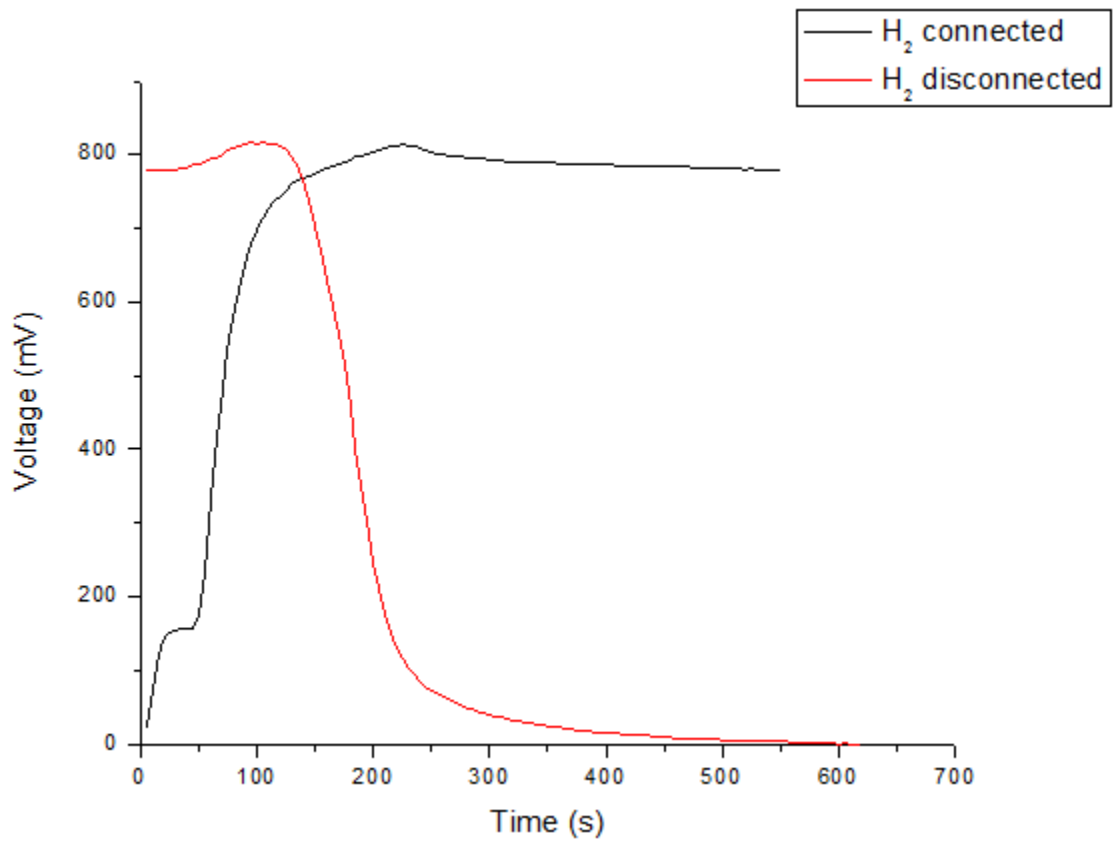


Figure 31. Voltage versus time curves of the SPI based fuel cell

The fuel cell voltage increased and become stable at nearly 800mV. The proton exchange chemical reaction needs time to happen (hydrogen arrived at the interface with the catalyst). The catalyst helps the reaction to continue as long as the reactants (hydrogen and oxygen) are provided. When the hydrogen was disconnected, the voltage of the PEMFC was not dropped immediately; it was still around at 800mV for nearly 100s, and then dropped gradually to zero after 400s. This situation can be explained by the chemical reaction; when the hydrogen connection was cut off, there was still some hydrogen in the gas channel of the fuel cell and the gas diffusion layer. It took 100s to deplete leftover hydrogen.

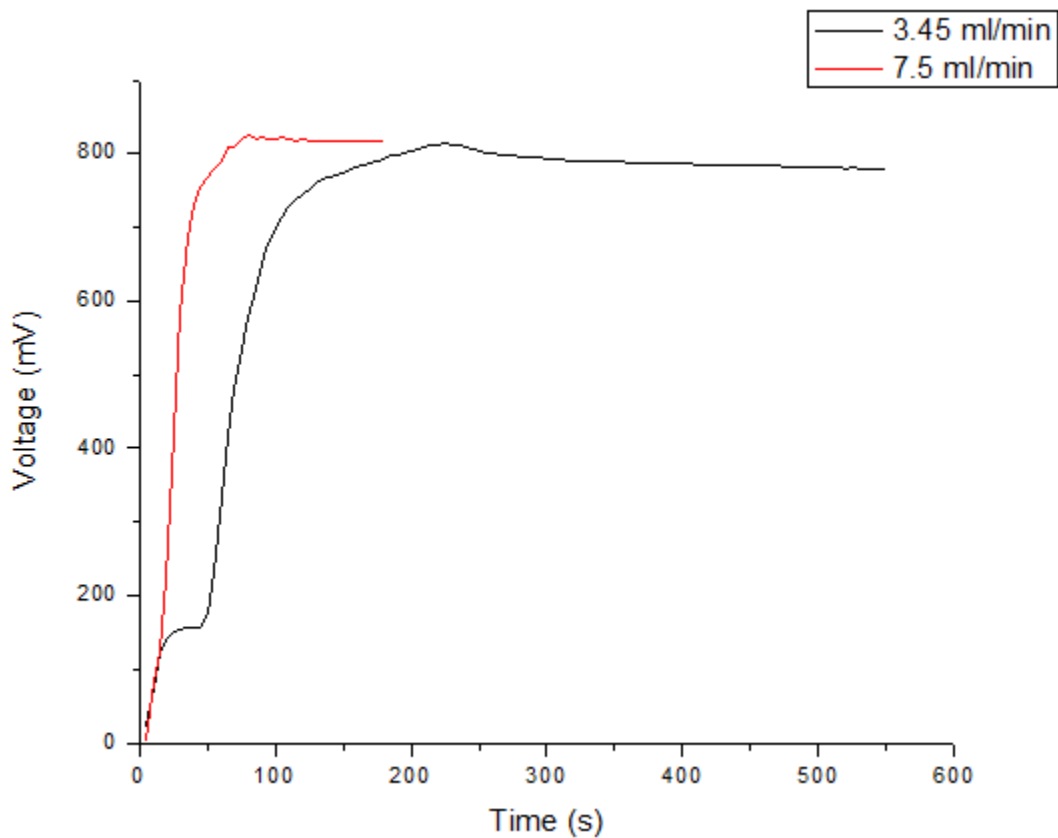


Figure 32. Voltage versus time curves of the SPI based fuel cell under two different H₂ flow rates

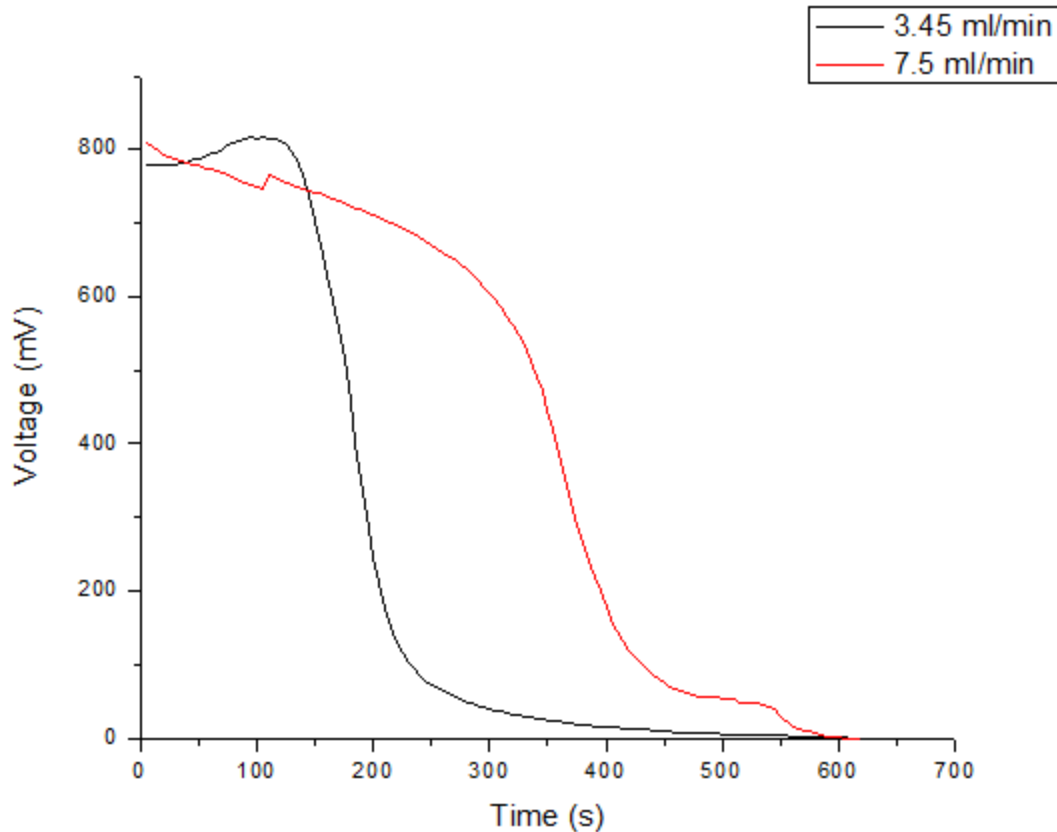


Figure 33. Voltage versus time curves of the SPI based fuel cell with hydrogen disconnected under two different H₂ flow rates

Figures 32 and 33 indicate the voltage versus time curve of the SPI based fuel cell under two different H₂ flow rate with hydrogen connected and disconnected, respectively. It can be stated that it takes different times to get the voltage of the fuel cell stable under two different hydrogen flow rates. It is obvious that the fuel cell under 7.5ml/min flow rate only needed nearly 100 seconds to become stable, which is much faster than under 3.45ml/min flow rate (nearly 200 seconds). The voltage of the fuel cell under 7.5ml/min flow rate was slightly higher than that of 3.45ml/min flow rate. Therefore, it can be concluded that hydrogen flow rate plays an important role in the SPI based MEA fuel cell. When the hydrogen was disconnected after reaching the

stability, although the voltage drop rate was not the same, two fuel cells nearly took the same time to cease the voltage generation. (550s and 600s)

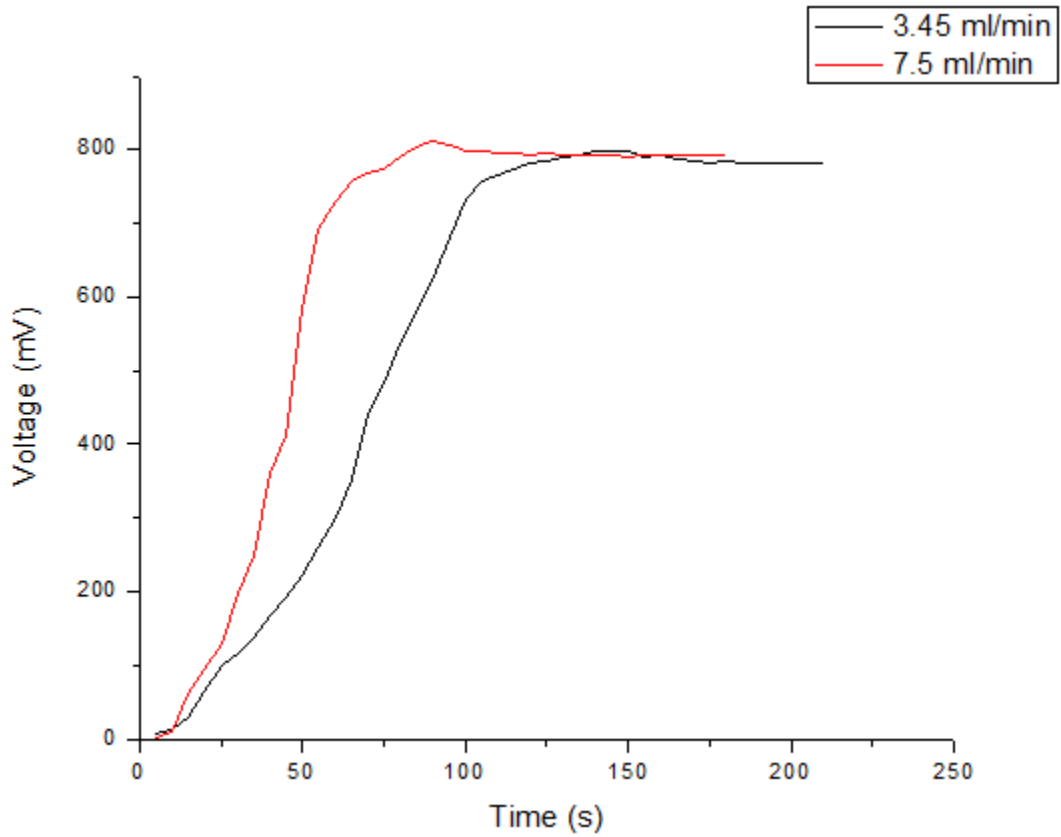


Figure 34. Voltage versus time curves of the Nafion® based fuel cell under two different H₂ flow rates

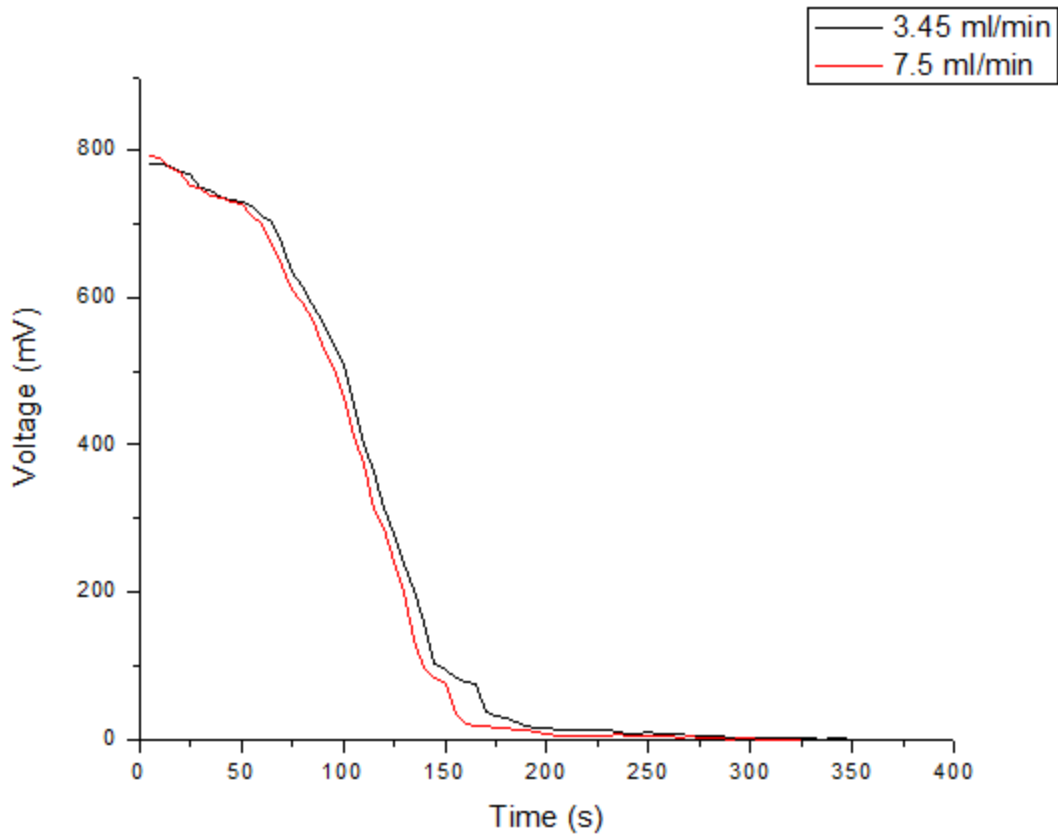


Figure 35. Voltage versus time curves of the Nafion® based fuel cell with hydrogen disconnected under two different H₂ flow rates

Figures 34 and 35 show the similar tests shown in Figures 32 and 33. The only difference between them is that the MEA is commercial Nafion® based MEA instead of the SPI based MEA. The same conclusions can be reached for the Nafion® based fuel cell. However, the Nafion® based fuel cell reached the stability earlier than the SPI based fuel cell (75s to 120s compared to 100s to 200s).

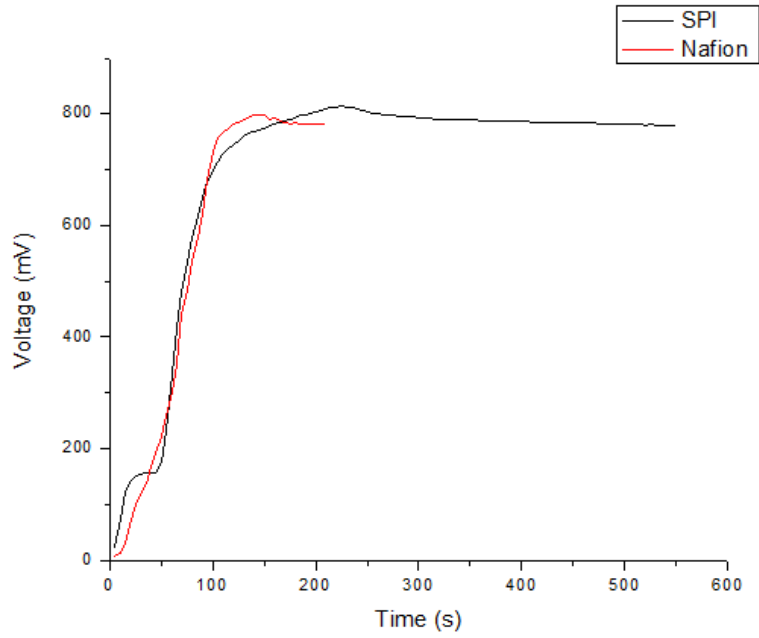


Figure 36. Voltage versus time curves of the fuel cells with different MEAs under the same hydrogen flow rate

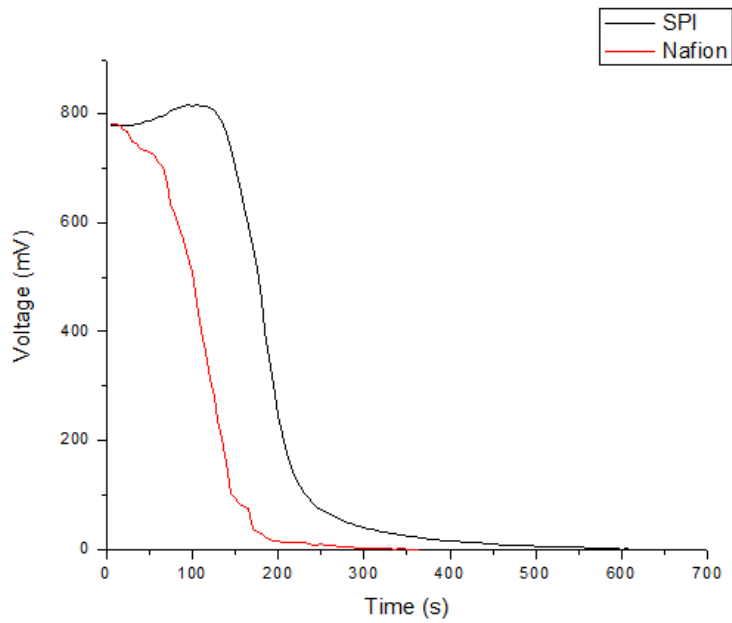


Figure 37. Voltage versus time curves of the fuel cells with different MEAs with hydrogen disconnected under the same hydrogen flow rate

Figures 36 and 37 compare the SPI and Nafion® based fuel cells under 3.45 ml/min hydrogen flow rate. Commercial Nafion® took only 120s to reach the voltage stability (780 mV), and the SPI based fuel cell took nearly 200s to reach 800mV. When the hydrogen disconnected, the voltage of Nafion® took 250s to drop to zero compared to 500s of the SPI based fuel cell.

It is obvious that the Nafion® based fuel cell is more suitable for mobile applications for its fast reaction to hydrogen connection or disconnection. However, it can also be concluded that the SPI based fuel cell has a higher potential to become a high performance fuel cell for stationary applications, in which the activation time is not important. Moreover, it can maintain higher voltage than the Nafion® based fuel cell under the same conditions. Most importantly, it has temperature-resistance over 120°C, which Nafion® cannot withstand.

Chapter Five

Future Developments in Synthesizing

The future development in synthesis will be briefly divided into four areas: in situ technique to raise the ionic conductivity, post-sulfonation to enhance the functional groups, cross-linking reaction to improve the mechanical properties and automatic solution casting to modify the membrane surface.

5.1. In Situ Technique

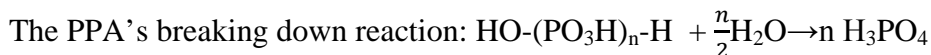
There are two important factors that have significant influences on the proton conductivity of the PEMs: their electrostatic interaction with ionic groups in polymer chains and their hydrophilic-channel structure. The interaction between water molecules and polymer chains can be quantitatively analyzed by examining the state of water. The state of water in hydrated membranes can be broadly classified into two groups, which are free water and bound water. Free water is known to act as a proton-carrying medium, whereas bound water is considered to help establish hydrogen bonds.

In polymer chemistry, in situ means "in the polymerization mixture." Basically, in situ processing can be considered as a chemical encapsulation technique that is very similar to interfacial coating. In situ technique may become one possible method to form in situ hybrid

membranes to increase water uptake in the membranes because the in situ sol-gel synthesis occurs predominantly in the hydrophilic channels of the membranes. The in situ phase inversion process: after polymerization the hot viscous SPI solution is added with the Polyphosphoric acids (PPA) solution. And then, the SPI solution is poured directly onto the glass dish from polymerization temperature to room temperature, which means that the SPI transforms from solution state to the gel state. PPA will hydrolyze to the phosphoric acid to finish the doping process, and as a result, a new hybrid membrane would be obtained.

Actually, the in situ process described above is more intricate and rather versatile than it appears. In the first step, when the PPA water solution is added to the SPI m-cresol solution, the two solution system transform from two individual to one integral sol-gel system, in which m-cresol and water are immiscible due to rule of polar similarity. M-cresol is continuous phase (matrix), water is disperse phase (particles) and the SPI copolymer is believed to act as an emulsifier that is located at the interface of the two phases and reduce the interfacial tension. The copolymers at interface are expected to stabilize morphology against coalescence. However, the system stays in a high temperature condition, where one chemical and two physical reactions are taking place simultaneously. The PPA is absorbing water to transform to phosphoric acid; m-cresol and water are vaporizing at different speeds. M-cresol is supposed to evaporate faster than water because the boiling point of water is higher than that of m-cresol. In this sol-gel system, as the three reactions continue, the percentages of different components change. At one point, the amount of water just becomes larger than the amount of m-cresol, and the phase conversion takes place, which means that the water becomes continuous phase, while m-cresol changes to disperse phase. At the same time, the phosphoric acid is dissolving into water which has a contact with the SPI at the interface – doping occurs. When all the m-cresol and water are evaporated

completely, just leaving the phosphoric acid and SPI copolymer, doping has made the phosphoric acid and the SPI bond together physically. Therefore, one PPA-SPI hybrid membrane is believed to be obtained.



5.2. Post-sulfonation

The common synthesis strategy of the materials which can substitute Nafion® is based on the sulfonation of previously obtained non-ionomeric polymer. Membranes produced on the basis of this approach are commercially available. Sulfonation compounds which are in typical use comprise of sulfur trioxide SO₃, chlorosulfonic acid ClSO₃H, sulfuryl chloride SO₂Cl₂ and for some compounds, sulfuric acid.

From analyzing the chemical structure of the SPI, it can be found that there is potential to introduce more sulfonate acid groups into the backbone by substituting the H atoms on the benzene ring or reacting with the carbon-carbon double bond. However, it is hard to introduce additional sulfonate acid groups when one has already been attached to the benzene ring, because sulfonate acid groups' passivation function decreases the benzene ring's activity. The only choice is to attach the sulfonate acid group to the carbon-carbon double bond. This route leads to the introduction of additional steps in the synthesis process.

Due to the degradation process, a decrease in the molecular weight of the polymer may be observed during sulfonation and the material obtained is usually not homogenous in terms of the sulfonic group density. The additional disadvantage of the compounds used is related to their high chemical aggressiveness. Thus, their application to the synthesis of PEMFC membranes should be limited.

To overcome the disadvantages listed above, new sulfonating agents are needed. Sodium hydrogen sulfite is a good candidate; it is considered as a weak sulfonating agent. The reaction is easy to understand: after the SPI's polymerization ends, sodium hydrogen sulfite will be added with 3 times weight water to the SPI copolymer. Giving it enough time, the sodium hydrogen sulfite will attack carbon-carbon double bond to attach the sulfonate acid group onto the backbone. The reaction temperature is supposed to be $103 \text{ }^{\circ}\text{C} \pm 2^{\circ}\text{C}$. If the temperature is higher, it could easily lead to decomposition of sulfonating agent, the reaction could not start. If the temperature is lower, the sulfonation reaction time will increase while the whole reaction may not be complete, and sulfonation rate will decrease; The reaction time should also be controlled around 1.5~2.5 hours. As the reaction time increases, the sulfonation rate increases marginally; on the other hand, as the reaction time decreases, the sulfonation reaction may not be complete, and sulfonation conversion rate also decreases.

Thus, by utilizing the post-sulfonation of the SPI membrane to increase the $-\text{SO}_3\text{H}$ end groups, the final proton conductivity of the PEMs is believed to be increased.

5.3. Cross-linking Reaction

It is essential to have proper proton conductivity through the sulfonated polymer membranes to maintain the efficiency of fuel cells. Typically, the sulfonated polymers with high degree of sulfonation exhibit much-improved proton-releasing ability owing to increasing amount of fixed ions within the sulfonated polymers and at the same time, increasing the formation of proton carrier in acidic water medium [36]. However, high sulfonation also results in excessive water swelling (water-solubility), which consequently makes the membranes life-span become less in fuel cell applications.

Accordingly, crosslinking could be a good solution to maintain a proper sulfonation level or water uptake content and, simultaneously, to enhance the mechanical properties. So far, many attempts have been made to crosslink various sulfonated polymer membranes such as polyimide, poly(vinyl alcohol) (PVA), sulfonated polyphosphazene, sulfonated poly(aryl sulfinate) / poly(aryl sulfonate), sulfonated poly(ether ether ketone), and sulfonated polystyrene. In most cases, crosslinking improved the mechanical properties and membrane stability; therefore, introducing cross-linking reagents onto the SPI may improve the mechanical properties lost by the previous post-sulfonation of the SPI copolymer.

Diols will be used as potential cross-linking reagents. Cross-linked chain length is believed to play an important role in the final polymer's properties. Cross-linked chain length and chain flexibility in rigid sulfonated polymers significantly affect the final morphology due to the formation of effective hydrophilic channels, which influence proton conductivity and water uptake. It also means that enhancement of PEM performance can be achieved by controlling the chain length of cross linker as well as chemical modification of the polymer backbone.

After the post-sulfonation reaction, the SPI copolymer will be dissolved with m-cresol again and then controlled amount of diols will be added to the solution. The mixture will be stirred and heated with controlled time and temperature until the cross-linking is complete. By introducing the cross-linking reagents, the SPI copolymer is supposed to form a 3D network molecule structure. Mechanical tests will be performed to compare the samples before and after the reaction.

5.4. Automatic Solution Casting

The SPI membrane obtained has a problem that its surface flatness is not good. A uniform surface is an important requirement of the membrane. Basically, this problem is caused by

solution casting – the membrane preparation method itself. Solution casting is an easy way to obtain a membrane after synthesizing the polymer, which costs little. However, it has two flaws: firstly, the surface structure of the membrane depends on the casting base – normally a plate glass or a petri dish. The shape of membrane is supposed to be the same as the shape of the casting base bottom. Therefore, when the casting base itself has a poor surface condition – glass depletion at some points or some tiny dirt on the surface, the final membrane’s surface is questionable. Secondly, the casting environment is hard to control. The casting temperature and pressure are crucial in this method; to get a good surface structure, the distribution of solution is supposed to be controlled precisely, which is hardly possible with pure solution casting.

Thereby, using a programmable automatic coating machine can help to solve the problem. I&J4000-LF RoHs bench top dispensing industrial robot in our lab is a good choice; it is ideal for many automatic dispensing applications and membrane casting (Figure 38). Its nozzle’s resolution is 20 microns (Figure 39) and interpolation is in all axes. By using the software, designing a dispensing program is possible. As a result, the concentration of the solution at every point can be controlled, which is believed to improve the molecular orientation on the membrane surface.

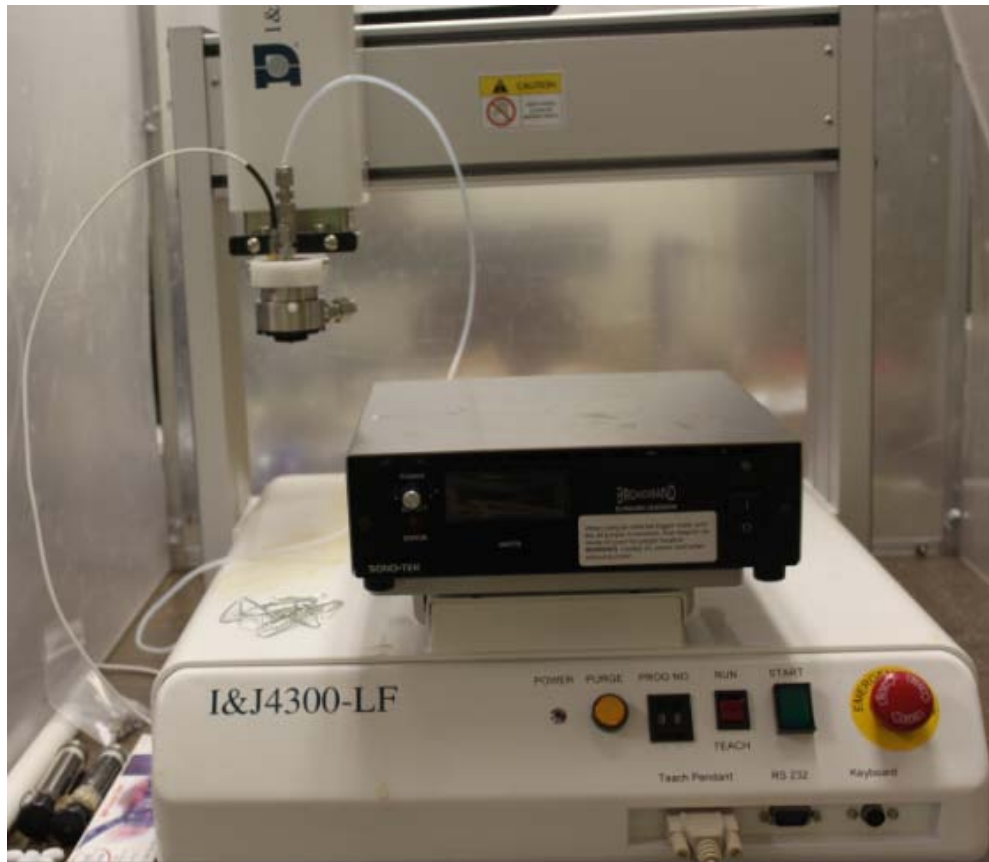


Figure 38. I&J4000-LF RoHs bench top dispensing industrial robot

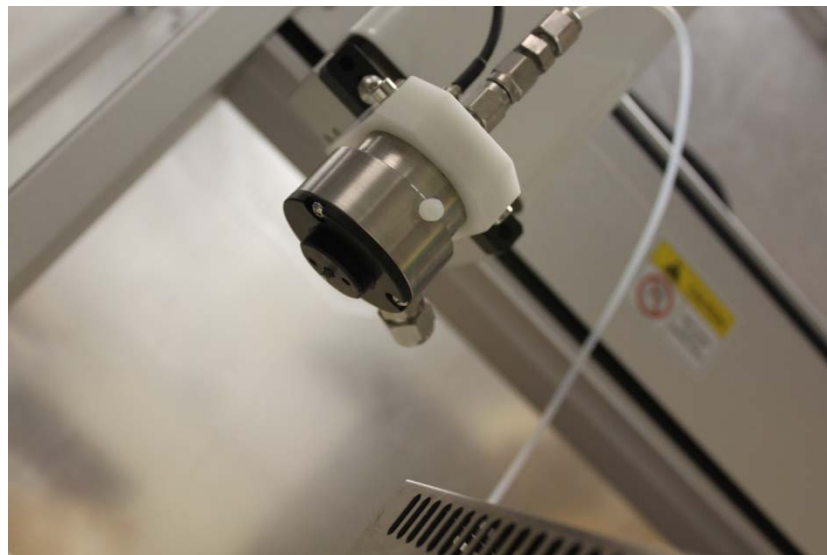


Figure 39. The nozzle in the dispensing industrial robot

Chapter Six

Conclusions

The SPI membranes were successfully fabricated using DSDSA and other commercial materials, which showed excellent solubility in m-cresol. TGA and DSC tests demonstrated that the SPI copolymers can be used in chemically stable proton exchange membranes at elevated temperatures, with mechanical stability. The SPI membrane based PEMFC worked successfully. The SPI membrane has a high potential to be used in a fuel cell for the stationary applications. It can maintain slightly higher voltage than Nafion® under the same conditions, and it has temperature-resistance over 120°C.

The SPI membrane has a good potential for relatively high temperature PEMFC applications. The proton conducting membrane developed is relatively low cost with good efficiency, which should help to promote the commercialization of the PEMFCs and broaden their application areas.

References

- [1] http://en.wikipedia.org/wiki/Carnot_cycle (accessed 5/24/2010)
- [2] http://www.epa.gov/OUST/fedlaws/publ_109-058.pdf (accessed 9/13/2010)
- [3] http://en.wikipedia.org/wiki/Fuel_cell (accessed 5/13/2010)
- [4] http://sitecoremedia.risoe.dk/research/fuel_cells/Images1/Forms/AllItems.aspx (accessed 8/29/2010)
- [5] L. Dan Milici, Mariana Milici, Radu Pentiu, Sorin Pohoata and Dinu Cirdei, Study of the Energetic Regime for a Fuel Cell Discharge (2008), 2nd International Conference On Modern Power Systems MPS 2008, 12-14 Nov 2008, CLUJ-NAPOCA, Romania.
- [6] http://www2.dupont.com/FuelCells/en_US/assets/downloads/dfc101.pdf (accessed 7/13/2010)
- [7] J. S. Lee, N. D. Quan, J. M. Hwang, S. D. Lee, H. Kim, H. Lee and H. S. Kim, Polymer Electrolyte Membranes for Fuel Cells, J. Ind. Eng. Chem., 12 (2006), 175-183.
- [8] M. Wilhelm, M. Jeske, R. Marschall, W. L. Cavalcanti, P. Tolle, C. Kohler, D. Koch, T. Frauenheim, G. Grathwohl, J. Caro and M. Wark, New proton conducting hybrid membranes for HT-PEMFC systems based on polysiloxanes and SO₃H-functionalized mesoporous Si-MCM-41 particles, J. Membr. Sci., 316 (2008), 164-175
- [9] J. Larminie, A. Dicks, Fuel Cell System Explained, Wiley, West Sussex, 2000.

- [10] S. Faure, N. Cornet, G. Gebel, R. Mercier, M. Pineri and B. Sillion, Sulfonated polyimides as novel proton exchange membranes for H₂/O₂ fuel cells, *New Materials for Fuel Cell and Modern Battery Systems II*, in *Proceedings of the 2nd International Symposium on New Materials for Fuel Cell and Modern Battery Systems*, Montreal, July 6–10 (1997), 818–827.
- [11] N. Cornet, O. Diat, G. Gebel, F. Jousse, D. Marsacq, R. Mercier and M. Pineri, Sulfonated polyimide membranes: a new type of ion-conducting membrane for electrochemical applications, *J. New Mater. Electrochem. Syst.*, 3 (1) (2000), 33–42.
- [12] V. Detallante, D. Langevin, C. Chappey, M. Metayer, R. Mercier and M. Pineri, Water vapor sorption in naphthalenic sulfonated polyimide membranes, *J. Membr. Sci.*, 190 (2) (2001), 227–241.
- [13] V. Detallante, D. Langevin, C. Chappey, M. Metayer, R. Mercier and M. Pineri, Kinetics of water vapor sorption in sulfonated polyimide membranes, *Desalination*, 148 (2) (2002), 333–339.
- [14] F. Piroux, E. Espuche, R. Mercier and M. Pineri, Water vapor transport mechanism in naphthalenic sulfonated polyimides, *J. Membr. Sci.*, 223 (1) (2003), 127–139.
- [15] C. Genies, R. Mercier, B. Sillion, R. Petiaud, N. Cornet, G. Gebel and M. Pineri, Stability study of sulfonated phthalic and naphthalenic polyimide structures in aqueous medium, *Polymer*, 42 (12) (2001), 5097–5105.
- [16] S. Besse, P. Capron, O. Diat, G. Gebel, F. Jousse, D. Marsacq, M. Pineri, C. Marestin and R. Mercier, Sulfonated polyimides for fuel cell electrode membrane assemblies (MEA), *J. New Mater. Electrochem. Syst.*, 5 (2) (2002), 109–112.

- [17] C. Genies, R. Mercier, B. Sillion, N. Cornet, G. Gebel, M. Pineri, Soluble sulfonated naphthalenic polyimides as materials for proton exchange membranes, *Polymer*, 42 (2) (2000) 359–373.
- [18] Y. Zhang, M. Litt, R. F. Savinell and J. S. Wainright, Molecular design considerations in the synthesis of high conductivity PEMs for fuel cells, *Polym. Prep. (Am. Chem. Soc., Div. Polym. Chem.)*, 40 (2) (1999), 480–481.
- [19] Y. Zhang, M. Litt, R.F. Savinell, J.S. Wainright, J. Vendramini, Molecular design of polyimides toward high proton conducting materials, *Polym. Prep. (Am. Chem. Soc., Div. Polym. Chem.)*, 41 (2) (2000) 1561–1562.
- [20] N. Gunduz and J. E. McGrath, Synthesis and characterization of sulfonated polyimides, *Polym. Prep. (Am. Chem. Soc., Div. Polym. Chem.)*, 41 (1) (2000), 182–183.
- [21] H. K. Shobha, M. Sankarapandian, T. E. Glass and J. E. McGrath, Sulfonated aromatic diamines as precursors for Polyimides for Proton Exchange Membranes, *Abstracts of Papers, American Chemical Society, 220th, 2000 (POLY-155)*.
- [22] B. R. Einsla, Y. T. Hong, Y. S. Kim, F. Wang, N. Gunduz and J. E. McGrath, Sulfonated naphthalene dianhydride based polyimide copolymers for proton-exchange-membrane fuel cells. I. Monomer and copolymer synthesis, *J. Polym. Sci., Part A: Polym. Chem.*, 42 (4) (2004), 862–874.
- [23] J. Fang, X. Guo, S. Harada, T. Watari, K. Tanaka, H. Kita, K. Okamoto, Novel sulfonated polyimides as polyelectrolytes for fuel cell application. 1. Synthesis, proton conductivity, and water stability of polyimides from 4,4'-diaminodiphenyl ether-2,2'-disulfonic acid, *Macromolecules*, 35 (24) (2002), 9022–9028.

- [24] X. Guo, J. Fang, T. Watari, K. Tanaka, H. Kita and K. Okamoto, Novel sulfonated polyimides as polyelectrolytes for fuel cell application. 2. Synthesis and proton conductivity of polyimides from 9,9'-bis(4-aminophenyl)fluorene-2,7-disulfonic acid, *Macromolecules*, 35 (17) (2002), 6707–6713.
- [25] T. Watari, J. Fang, K. Tanaka, H. Kita, K. Okamoto and T. Hirano, Synthesis, water stability and proton conductivity of novel sulfonated polyimides from 4,4'-bis(4-aminophenoxy)biphenyl-3,3'-disulfonic acid, *J. Membr. Sci.*, 230 (2004), 111–120.
- [26] Y. Yin, J. Fang, Y. Cui, K. Tanaka, H. Kita and K. Okamoto, Synthesis, proton conductivity and methanol permeability of a novel sulfonated polyimide from 3-(2',4'-diaminophenoxy)propane sulfonic acid, *Polymer*, 44 (16) (2003), 4509–4518.
- [27] Y. Yin, J. Fang, H. Kita and K. Okamoto, Novel sulfoalkoxylated polyimide membrane for polymer electrolyte fuel cells, *Chem. Lett.*, 32 (4) (2003), 328–329.
- [28] K. Okamoto, Sulfonated polyimides for polymer electrolyte membrane fuel cell, *J. Photopolym. Sci. Technol.*, 16 (2), (2003), 247–254.
- [29] H. K. Shobha, M. Sankarapandian, T. E. Glass and J. E. McGrath, Synthesis and characterization of sulfonated poly(arylene ether)s based on phosphine oxide for fuel-cell applications., *Polym. Prepr.*, 41 (2000), 1298.
- [30] O. J. Savadogo, Emerging membranes for electrochemical systems: (I) solid polymer electrolyte membranes for fuel cell systems, *New Mater. Electrochem. Syst.*, 1 (1998), 47.
- [31] C. Genies, R. Mercier, B. Sillion, N. Cornet, G. Gebel and M. Pineri, Stability study of sulfonated phthalic and naphthalenic polyimide structures in aqueous medium, *Polymer*, 42 (2001), 359.

- [32] N. Cornet, O. Diat, G. Gebel, F. Jousse, D.Marsacq, R. Mercier and M. Pineri, Sulfonated polyimide membranes: a new type of ion-conducting membrane for electrochemical applications, *J. New Mater. Electrochem. Syst.*, 3 (2000), 33.
- [33] http://www.fluent.com/solutions/fuel_cells/app13.htm (accessed 9/24/2010)
- [34] http://www.marklines.com/ja/amreport/rep347_200502.jsp (accessed 9/24/2010)
- [35] Y. S. Kim, L. Dong, M. A. Hickner, T. E. Glass, V. Webb and J. E. McGrath, State of water in disulfonated poly(arylene ether sulfone) copolymers and a perfluorosulfonic acid copolymer (Nafion®) and its effect on physical and electrochemical properties, *Macromolecules* 36 (2003), 6281.
- [36] Y. Su, Y. Liu, Y. Sun, J. Lai, B. Liu and M.D. Guiver, Proton exchange membranes modified with sulfonated silica nanoparticles for direct methanol fuel cells, *J. Membr. Sci.*, 296 (2007), 21.
- [37] D.H. Kim and S.C. Kim, Transport properties of polymer blend membranes of sulfonated and nonsulfonated polysulfones for direct methanol fuel cell application, *Macromol. Res.*, 16 (2008), 457.
- [38] M. Saito, N. Arimura, K. Hayamizu and T. Okdada, Mechanisms of ion and water transport in perfluorosulfonated ionomer membranes for fuel cells, *J. Phys. Chem. B*, 108 (2004), 16064.
- [39] Y. Fu, A. Manthiram and M.D. Guiver, Blend membranes based on sulfonated poly(ether ether ketone) and polysulfone bearing benzimidazole side groups for proton exchange membrane fuel cells, *Electrochem. Commun.*, 8 (2006), 1386.
- [40] J. Choi, D. H. Kim, H. K. Kim, C. Shin, S. C. Kim, Polymer blend membranes of sulfonated poly(arylene ether ketone) for direct methanol fuel cell, *J. Membr. Sci.*, 310 (2008), 384.

- [41] T. A. Zawodzinski, C. Derouin, S. Radzinski, R. J. Sherman, V. T. Smith, T. E. Springer and S. Gottesfeld, Water uptake by and transport through Nafion® 117 membranes, J. Electrochem. Soc., 140 (1993), 1041.
- [42] S. Y. So, Y. T. Hong, S. C. Kim and S. Y. Lee, Control of water-channel structure and state of water in sulfonated poly(arylene ether sulfone)/diethoxydimethylsilane in situ hybridized proton conductors and its influence on transport properties for DMFC membranes, J. Membr. Sci., 346 (2010), 131.
- [43] P. D. Beattie, F. P. Orfino, V. I. Basura, K. Zychowska, J. Ding, C. Chuy, J. Schmeisser and S. Holdcroft, Ionic conductivity of proton exchange membranes, J. Electroanal. Chem., 503 (2001), 45.
- [44] http://www2.dupont.com/FuelCells/en_US/assets/downloads/dfc101.pdf (accessed 9/5/2010)
- [45] L. Isikel, I. Gocek and S. Adanur, Design and characterization of nonwoven fabrics for gas diffusion layer in polymer electrolyte membrane fuel cell, J. Textile. Inst., 101 (2010), 1006–1014.